

## NOGAPS-ALPHA Simulations of the 2002 Southern Hemisphere Stratospheric Major Warming

DOUGLAS R. ALLEN

*Remote Sensing Division, Naval Research Laboratory, Washington, D.C.*

LAWRENCE COY, STEPHEN D. ECKERMANN, AND JOHN P. MCCORMACK

*E. O. Hulburt Center for Space Research, Naval Research Laboratory, Washington, D.C.*

GLORIA L. MANNEY

*Jet Propulsion Laboratory, California Institute of Technology, Pasadena, California, and New Mexico Highlands University, Las Vegas, New Mexico*

TIMOTHY F. HOGAN AND YOUNG-JOON KIM

*Marine Meteorology Division, Naval Research Laboratory, Monterey, California*

(Manuscript received 29 September 2004, in final form 8 July 2005)

### ABSTRACT

A high-altitude version of the Navy Operational Global Atmospheric Prediction System (NOGAPS) spectral forecast model is used to simulate the unusual September 2002 Southern Hemisphere stratospheric major warming. Designated as NOGAPS-Advanced Level Physics and High Altitude (NOGAPS-ALPHA), this model extends from the surface to 0.005 hPa (~85 km altitude) and includes modifications to multiple components of the operational NOGAPS system, including a new radiative heating scheme, middle-atmosphere gravity wave drag parameterizations, hybrid vertical coordinate, upper-level meteorological initialization, and radiatively active prognostic ozone with parameterized photochemistry. NOGAPS-ALPHA forecasts (hindcasts) out to 6 days capture the main features of the major warming, such as the zonal mean wind reversal, planetary-scale wave amplification, large upward Eliassen–Palm (EP) fluxes, and splitting of the polar vortex in the middle stratosphere. Forecasts beyond 6 days have reduced upward EP flux in the lower stratosphere, reduced amplitude of zonal wavenumbers 2 and 3, and a middle stratospheric vortex that does not split. Three-dimensional EP-flux diagnostics in the troposphere reveal that the longer forecasts underestimate upward-propagating planetary wave energy emanating from a significant blocking pattern over the South Atlantic that played a large role in forcing the major warming. Forecasts of less than 6 days are initialized with the blocking in place, and therefore are not required to predict the blocking onset. For a more thorough skill assessment, NOGAPS-ALPHA forecasts over 3 weeks during September–October 2002 are compared with operational NOGAPS 5-day forecasts made at the time. NOGAPS-ALPHA forecasts initialized with 2002 operational NOGAPS analyses show a modest improvement in skill over the NOGAPS operational forecasts. An additional, larger improvement is obtained when NOGAPS-ALPHA is initialized with reanalyzed 2002 fields produced with the currently operational (as of October 2003) Naval Research Laboratory (NRL) Atmospheric Variational Data Assimilation System (NAVDAS). Thus the combination of higher model top, better physical parameterizations, and better initial conditions all yield improved forecasting skill over the NOGAPS forecasts issued operationally at the time.

---

*Corresponding author address:* Douglas Allen, Dept. of Physics and Astronomy, Dordt College, 498 Fourth Avenue NE, Sioux Center, IA 51250.

E-mail: dallen@dordt.edu

## 1. Introduction

A research project at the Naval Research Laboratory (NRL) has extended the Navy Operational Global Atmospheric Prediction System (NOGAPS) spectral forecast model from its current 1.0-hPa upper boundary to include a fully resolved prognostic middle atmosphere (Eckermann et al. 2004). This work is ongoing; the goal is to progressively transition aspects of this new NOGAPS-Advanced Level Physics and High Altitude (NOGAPS-ALPHA) to the Fleet Numerical Meteorological and Oceanographic Center (FNMOC) as part of a next-generation high-altitude NOGAPS that improves numerical weather prediction (NWP) at all levels. NOGAPS-ALPHA has been used in several studies to date. An early experimental extended-top (0.1 hPa) version of NOGAPS was used by Kim and Hogan (2004) to investigate forecast sensitivity to various drag mechanisms. McCormack et al. (2004) used the new prognostic ozone capability of NOGAPS-ALPHA to hindcast Arctic stratosphere ozone during January 2003 and compared it with aircraft data and ozone forecasts and analyses from the European Centre for Medium-Range Weather Forecasts (ECMWF) Integrated Forecast System (IFS). Coy et al. (2005) simulated a Southern Hemisphere minor stratospheric warming and mesospheric cooling that occurred in August 2002.

This paper builds on the previous work by verifying NOGAPS-ALPHA forecasts (we use the term “forecast” here although all NOGAPS-ALPHA runs here were made as hindcasts) of the September 2002 Southern Hemisphere (SH) major warming. This event provides a challenging test case for the model. The highly active 2002 SH winter culminated in September with rapid enhancement of zonal waves 1, 2, and 3 in the stratospheric geopotential height that accompanied the splitting of the winter polar vortex in the middle and upper stratosphere, reversal of the polar night jet, and record warming of the polar region in late September (Allen et al. 2003; Sinnhuber et al. 2003; Weber et al. 2003; also see special issue of the *Journal of Atmospheric Science*, vol. 62, no. 3, hereinafter *JAS* 2005). Similar to Northern Hemisphere (NH) sudden warmings, strong nonlinear wave–wave interaction occurred, and the vortex may have experienced a cumulative preconditioning process that facilitated the major warming (Baldwin et al. 2003; Krüger et al. 2005). However, mechanistic model simulations by Manney et al. (2005a) suggest that, because of unusually strong upper-tropospheric/lower-stratospheric planetary wave forcing, stratospheric preconditioning (in the conventional sense of a more poleward jet) was not necessary to produce this major warming. A key to understanding

the 2002 SH warming is to determine the source of this large upward flux of planetary wave activity in the upper troposphere/lower stratosphere, which preceded the warming. Observations showed that the 100-hPa poleward eddy heat flux immediately preceding the warming was much larger than that seen in any previous year (Allen et al. 2003; Sinnhuber et al. 2003; Weber et al. 2003; Harnik et al. 2005; Newman and Nash 2005; Scaife et al. 2005).

The source of this wave energy flux may be related to tropospheric blocking. Observational studies have identified a connection between stratospheric warmings and tropospheric blocking events in both the Northern and Southern Hemispheres (e.g., Quiroz 1986; Mechoso et al. 1988). Niishi and Nakamura (2004, hereinafter NN04) argue that the 2002 SH major warming was forced by large planetary wave fluxes emanating from a tropospheric blocking ridge over the South Atlantic. This ridge formed as part of a Rossby wave train, which NN04 argue originated from enhanced deep convection around the South Pacific convergence zone. It is therefore of interest to examine whether forecast models that have a well-resolved troposphere and stratosphere are able to predict the blocking in conjunction with the subsequent stratospheric major warming.

In fact, this stratospheric major warming was predicted up to about a week in advance by operational weather forecasts issued by both the National Centers for Environmental Prediction’s (NCEP) Global Forecast System (GFS) (J. Derber 2003, personal communication) and the ECMWF’s IFS (Simmons et al. 2005). Studies have shown that the predictive skill of NWP models is better in the lower stratosphere than in the midtroposphere (e.g., Waugh et al. 1998; Lahoz 1999). Forecast skill in the stratosphere depends on many factors, including flow history, flow structure, vertical resolution in the stratosphere, location of highest model full and half levels, initialization errors, and tropospheric forecasting errors (Mechoso et al. 1985, 1986; Lahoz 1999). Targeted studies of specific warming events show that in some cases the warming can be predicted up to several weeks in advance (Mukougawa and Hirooka 2004), while in other cases, particularly rapidly evolving “wave 2”-type warmings, the predictability is on the order of a week or less (Mechoso et al. 1985; Simmons et al. 2005).

Given the observed relationship between tropospheric blocking and stratospheric warmings, the success of forecasting stratospheric warmings may depend strongly on the success of forecasting blocking conditions in the lower atmosphere. NWP models often have trouble forecasting the onset of blocking events, particularly in the Southern Hemisphere (Tibaldi et al.

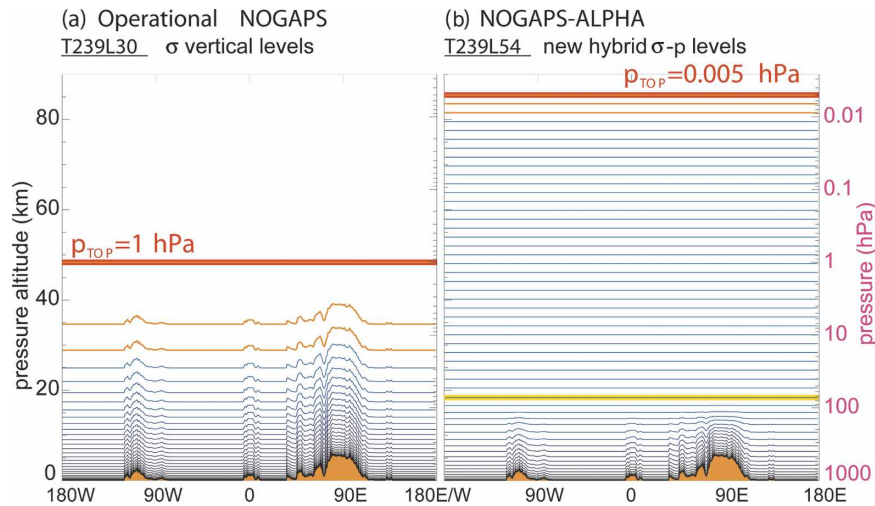


FIG. 1. NOGAPS vertical levels around  $34.5^{\circ}\text{N}$  lat for (a) operational 30-level (L30) model with top at 1 hPa and (b) new NOGAPS-ALPHA 54-level (L54) model with top at 0.005 hPa. Model layers near the top boundary where enhanced numerical damping and diffusion are applied are highlighted in orange. Yellow curve shows the first purely isobaric stratospheric half level at  $\sim 72.6$  hPa.

1994). Forecasts initialized with blocked conditions in place usually have better performance than those initialized prior to blocking onset. In this paper, we analyze NOGAPS-ALPHA forecasts for varying durations and initial conditions to try to determine if there is any connection between the skill of forecasting the observed major warming and the skill of forecasting tropospheric blocking. This will also provide an independent test of the NN04 hypothesis for the warming's origin as well as further validation for the NOGAPS-ALPHA model.

The paper is organized as follows. Section 2 provides an overview of NOGAPS-ALPHA and discusses the model configurations and initialization fields used in this study. Section 3 presents NOGAPS-ALPHA forecasts of the stratospheric major warming and associated tropospheric blocking for different forecast durations. In section 4 we quantify the forecast skill of NOGAPS-ALPHA using standard skill diagnostics, comparing with operational NOGAPS forecasts over a 3-week period during September and October 2002. Section 5 discusses and summarizes our major findings.

## 2. NOGAPS-ALPHA model description

### a. Operational NOGAPS model

NOGAPS is the Department of Defense's high-resolution global NWP system. Hogan and Rosmond (1991) and Hogan et al. (1991) provide a detailed description of the global forecast model. Briefly, NOGAPS is a global Eulerian spectral model in the

horizontal and uses a generalized vertical coordinate within an energy-conserving vertical finite-difference formulation. The operational model runs at the FN-MOC with a horizontal resolution of T239 and 30 model levels with a top pressure half level of 1 hPa (see Fig. 1a). The model's dynamical variables are relative vorticity, divergence, virtual potential temperature, specific humidity, and terrain (surface) pressure. The model is central in time with a semi-implicit treatment of gravity wave propagation and uses Robert (Asselin) time filtering. The current operational model's physics packages include a bulk Richardson number-dependent vertical mixing scheme (Louis et al. 1982); a time-implicit Louis surface flux parameterization (Louis 1979); flow-blocking and orographic gravity wave drag (Webster et al. 2003); shallow cumulus mixing of moisture, temperature, and winds (Tiedtke 1984); the Emanuel cumulus parameterization (Emanuel and Zivkovic-Rothman 1999; Peng et al. 2004); convective, stratiform, and boundary layer cloud parameterizations (Slingo 1987; Teixeira and Hogan 2002); and a shortwave and longwave radiation scheme (Harshvardhan et al. 1987).

### b. NOGAPS-ALPHA model

Here we summarize the major developments in NOGAPS-ALPHA. More complete descriptions are provided in Eckermann et al. (2004) and McCormack et al. (2004). NOGAPS-ALPHA replaces the current sigma coordinate with a hybrid sigma-pressure coordinate that transitions from terrain-following near the

surface to pure pressure levels at  $\sim 72.6$  hPa; the hybrid coordinate has been shown to improve middle-atmosphere simulations (e.g., Trenberth and Stepaniak 2002). Our initial T239L54 model (Fig. 1b) uses a hybrid formulation that produces uniformly smooth transitions to constant pressure height thicknesses in the stratosphere over arbitrary topography (Eckermann et al. 2004) and adopts constant pressure height thicknesses of  $\sim 2$  km throughout the rest of the middle atmosphere. This uniform vertical resolution is similar to current choices adopted for the ECMWF IFS.

A new family of physics packages was needed to adequately simulate the new upper altitudes of the prognostic NOGAPS-ALPHA atmosphere. We have replaced the operational radiation scheme (Harshvardhan et al. 1987) with the "CLIRAD" shortwave and longwave radiation schemes described by Chou and Suarez (2002) and Chou et al. (2001), respectively. CLIRAD improves the radiative heating and cooling calculations at all levels, but significantly improves the middle atmosphere. NOGAPS-ALPHA also currently includes six gravity wave drag (GWD) parameterizations, which are being tested and can all be either activated or deactivated for a given run, as well as a generalized Rayleigh friction scheme for use as a simpler proxy for mesospheric GWD (Eckermann et al. 2004). For the polar SH winter forecasts examined in this paper, only orographic GWD (OGWD) should be significant. We parameterized OGWD in the runs reported here using the Palmer et al. (1986) scheme (with its parameterized GWD applied only up to 150 hPa), since this same scheme was used operationally in NOGAPS throughout 2002. We deactivated the other five GWD schemes. Note that all NOGAPS-ALPHA and NOGAPS-ops (the archived FNMOC operational forecasts) forecasts were performed using silhouette orography, while the currently operational NOGAPS transitioned to mean orography in November 2003.

We have also introduced and continue to develop a new three-dimensional (3D) prognostic ozone capability. The current formulation is described by Eckermann et al. (2004), who also show some preliminary NOGAPS-ALPHA total ozone hindcasts based on these schemes for the 2002 SH warming, and by McCormack et al. (2004), who provide preliminary validation of the performance of prognostic ozone via hindcast runs in the Arctic during January 2003. Briefly, NOGAPS-ALPHA now ingests analyzed 3D ozone mixing ratio fields and advects them spectrally as a new prognostic chemistry variable. The ozone initialization is based currently on ozone analyses from the National Aeronautics and Space Administration's (NASA) Global Modeling and Assimilation Office (Riishoj-

gaard et al. 2000; Stajner et al. 2001) up to 1 hPa and an ozone climatology from 1 to 0.005 hPa. We have incorporated several existing linearized ozone photochemistry schemes (Cariolle and Déqué 1986; McLinden et al. 2000) for chemical updating of these fields and are currently developing a new scheme based on output from sensitivity experiments with NRL's two-dimensional model (McCormack et al. 2004). All runs in this paper use the Cariolle and Déqué (1986) photochemistry scheme and feed the 3D prognostic ozone into the shortwave and longwave radiation calculations.

For initialization of the meteorological fields, we use a "cold start" procedure in which analyzed winds and geopotential heights on pressure surfaces are interpolated to the model levels (temperature is calculated internally from the heights using hydrostatic balance). During September 2002, the NOGAPS operational analysis was based on a multivariate optimal interpolation (MVOI) system (Goerss and Phoebus 1992), with assimilated meteorological fields at FNMOC extending to 10 hPa. An experimental "STRATOI" product was also issued at the time, based mostly on Television Infrared Observation Satellite (TIROS) Operational Vertical Sounder (TOVS) radiances from the Microwave Sounding Unit, which yielded additional initialization fields for winds and geopotential heights up to 0.4 hPa. Unfortunately, the STRATOI fields were not archived during this period, so we have opted instead to use ECMWF IFS analyzed winds and layer thicknesses for initializing the region from 10 to 1 hPa. Given our current upper boundary of 0.005 hPa, we have developed a generalized upper-level initialization scheme that extrapolates topmost initialization winds and geopotentials by progressively relaxing them with increasing altitude to seasonally varying 2D climatological values from either the 1986 Committee on Space Research (COSPAR) International Reference Atmosphere (CIRA; Fleming et al. 1990) or the Upper Atmosphere Research Satellite (UARS) Reference Atmosphere Project (URAP; Swinbank and Orland 2003): see Eckermann et al. (2004) for details. In all the forecasts in this paper, initialization was based on relaxing to URAP winds and CIRA geopotentials, since URAP temperatures only extend to  $\sim 60$  km. After the pressure-level fields are interpolated to the model grid, the fields are run through a nonlinear normal-mode filter (Errico et al. 1988) before starting the forecast.

### *c. Initialization fields and model hindcasting configurations*

The two NOGAPS models we use in this paper are depicted in Fig. 1. We refer to the T239L30 model hereafter as "NOGAPS," since this same model resolution

is still (as of March 2005) used operationally at FNMOC (note that NOGAPS transitioned from T159L24 to T239L30 at FNMOC on 18 September 2002, just a week before the major warming). We do not rerun the NOGAPS model configuration in hindcast mode here, but instead use the archived 5-day forecast fields it generated operationally at FNMOC during this period. We denote hereafter by “ALPHA” the T239L54 NOGAPS-ALPHA model (Fig. 1b), which we run here in hindcast configurations using different operational analysis fields.

We shall refer to the archived operational MVOI fields as the “operational analysis,” or “ops” for short, NOGAPS-ops designates forecasts produced by the T239L30 model initialized with MVOI operational analysis fields. However, one should keep in mind that this describes an operational situation in 2002 that no longer holds today, since the MVOI system was replaced at FNMOC in 2003 by a new system, the NRL Atmospheric Variational Data Assimilation System (NAVDAS), which is based on 3D variational data assimilation (3DVAR; Daley and Barker 2001).

To test the impact of NAVDAS on NOGAPS-ALPHA forecasts in the troposphere and stratosphere, our “ALPHA” (T239L54) model runs are initialized not only with the archived “ops” fields, but also with a 2002 reanalysis that was performed using the currently operational NAVDAS, with pressure-level data extending up to 4 hPa. This reanalysis also includes radiance assimilation in place of National Environmental Satellite, Data, and Information Service (NESDIS) temperature retrievals; this capability became operational at FNMOC in June 2004 [see Baker et al. (2005) for details]. We denote these reanalysis fields “rean,” with the understanding that they are a good representation of what the current operational assimilation system might have produced had it been running operationally during 2002. For each of these ALPHA hindcast runs, we use the “cold start” procedure described earlier. These hindcast NWP configurations are denoted ALPHA-ops and ALPHA-rean.

### 3. NOGAPS-ALPHA forecasts of the stratospheric major warming and tropospheric blocking

#### a. Description of diagnostics

In this section we examine dynamical features of the 2002 SH major warming event in the middle stratosphere (10 hPa), lower stratosphere (100 hPa), and troposphere (500 hPa). We compare NOGAPS-ALPHA forecasts of varying durations with the NOGAPS re-

analyzed fields (rean) to determine how well the new model can predict the salient features of the event. We show only ALPHA-rean forecasts here, while ALPHA-ops and NOGAPS-ops forecasts are examined in section 4.

We will start by examining the synoptic evolution of the stratospheric geopotential height, zonal mean wind and temperature, and amplitude and phase of large-scale planetary waves 1, 2, and 3. Next, we will look at the zonally averaged Eliassen–Palm (EP) flux, which is conserved (nondivergent) for nondissipating planetary waves, and thus it is a fundamental measure of wave activity whose vector direction indicates the group velocity of waves in the meridional plane (Andrews et al. 1987). We will focus on the upward component of the EP-flux vector, which is proportional to the eddy heat flux  $\overline{v'T'}$ , where  $v'$  and  $T'$  are meridional wind and temperature departures from zonal mean, respectively, and overbar denotes zonal averaging. In the troposphere, we will compute the three-dimensional EP flux based on the work of Plumb (1986), in which small-amplitude, quasigeostrophic eddies, on a slowly varying time-mean flow, are shown to be associated with a conserved measure of wave activity flux. This three-dimensional EP flux is based on eddy statistics calculated with respect to a time-averaged mean state. We calculate the 3D flux separately for the analysis (in our case the NOGAPS reanalysis discussed in section 2c) and for the NOGAPS-ALPHA forecasts using daily deviations of the geopotential heights and winds from the analyzed September 2002 monthly mean. While the Plumb (1986) formulation is based on quasigeostrophic winds, here we use the full winds generated by the analysis and forecasts. We compare the analyzed and forecast wave activity fluxes, which allow us to pinpoint the location and quantify the magnitude of significant propagation of planetary wave energy from the troposphere into the stratosphere.

#### b. Analyses and forecasts in the middle stratosphere (10 hPa)

A conspicuous feature of the 2002 SH major warming was the splitting of the polar vortex in the middle stratosphere (JAS 2005). Figure 2 shows SH polar orthographic maps of the 10-hPa geopotential height on 26 September 2002 (note: all forecasts and analyses in this paper are plotted at 1200 UTC) from the NOGAPS reanalysis (hereinafter called “the analysis”) along with ALPHA-rean forecasts initialized on 16, 18, 20, and 22 September. Hereinafter, we will denote these forecasts by R16, R18, R20, and R22, respectively. The analyses leading up to 26 September (not shown) display a nearly circular polar vortex on 16 September that rap-

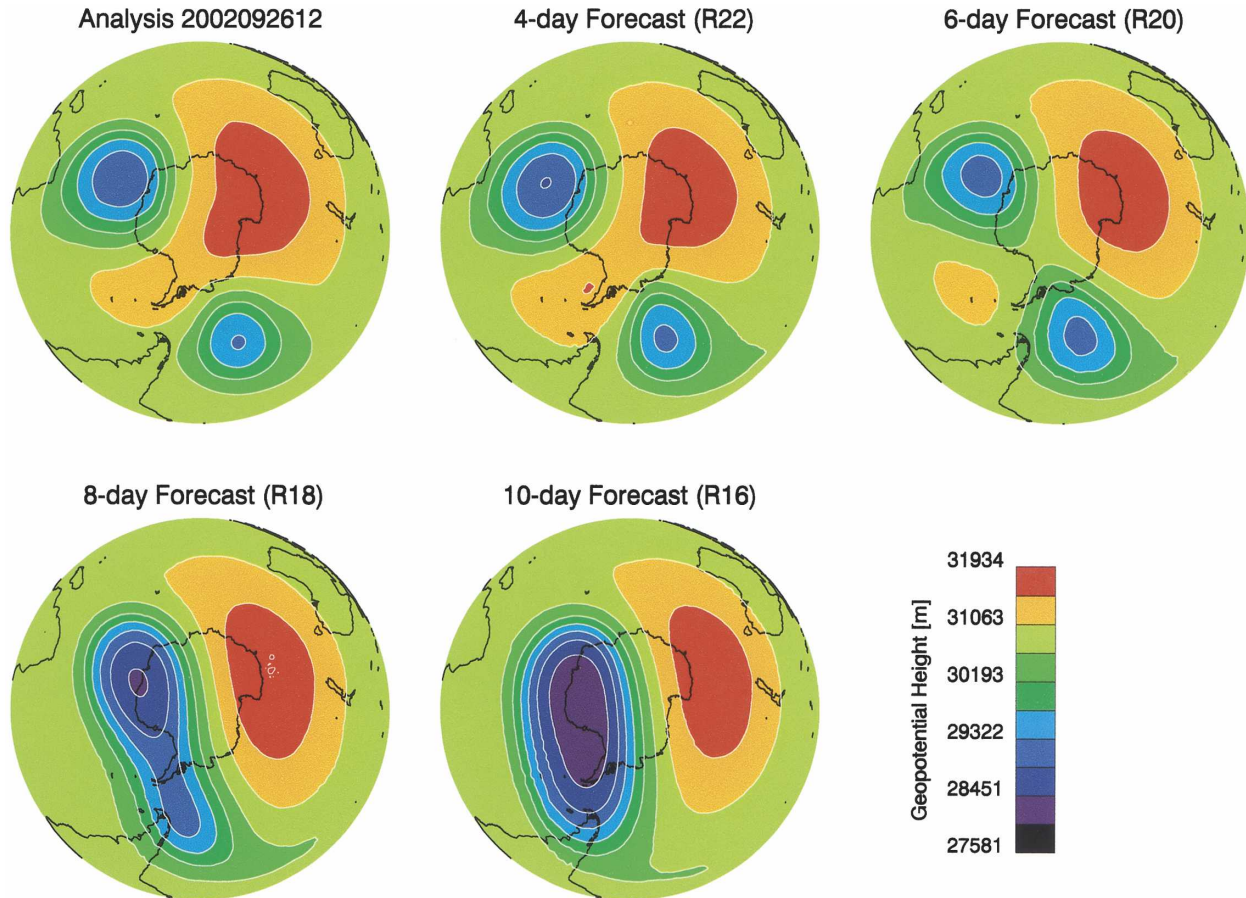


FIG. 2. Geopotential height at 10 hPa ( $\sim 32$  km) over the SH for 26 Sep 2002 for the analysis (NOGAPS reanalysis) and ALPHA-rean forecasts initialized 22, 20, 18, and 16 Sep 2002. All forecasts and analyses are plotted for 1200 UTC.

idly evolves into a strong zonal wave 1 pattern, with a strengthening anticyclone south of Australia, the so-called Australian high (Harvey et al. 2002). The middle of the vortex starts to become “pinched” by two opposing ridges so that by 24 September two distinct cyclonic cells develop within the vortex. Figure 2 shows that on 26 September the polar vortex splits into two pieces (here we identify a “split” vortex as one in which there are no closed geopotential height contours surrounding both vortex cells). Although split polar vortices have occurred during a number of strong major warming events in the NH (Andrews et al. 1987), this is the first time the SH vortex has ever been observed to split at 10 hPa so early in the year.

R22 (4-day forecast) nicely captures the splitting of the vortex at this level. R20 (6-day forecast) also shows a split vortex, but the separation of the two vortex lobes is not as distinct as in the analysis. Although R18 and R16 (8- and 10-day forecasts) show an elongated vortex, the vortex core does not split, but remains in a strong wave 1 pattern. This is consistent with results

from Simmons et al. (2005), who showed that operational ECMWF forecasts beyond 7 days were not able to capture the complete splitting of the vortex at 10 hPa.

The synoptic plots in Fig. 2 suggest rapid changes in the zonal mean conditions during the event. Figure 3 provides the evolution of zonal mean wind, temperature, and eddy heat flux from 15 to 30 September for the analysis (top row) and forecasts R20, R18, and R16. The reversal of winds to easterlies during the major warming is seen in the analysis at 10 hPa. R20 nicely captures the wind reversal to easterly starting at the pole on 22 September and eventually encompassing all latitudes from  $30^\circ$  to  $90^\circ$ S. R16 and R18 both show a region of easterlies developing near the pole, but the core of the polar jet remains westerly.

The analyses show a reversal of the meridional temperature gradient (middle column of Fig. 3) on 21 September due to rapid warming of the polar region. The forecasts all show reversal of the temperature gradient around 21 September. However, the magnitude of the

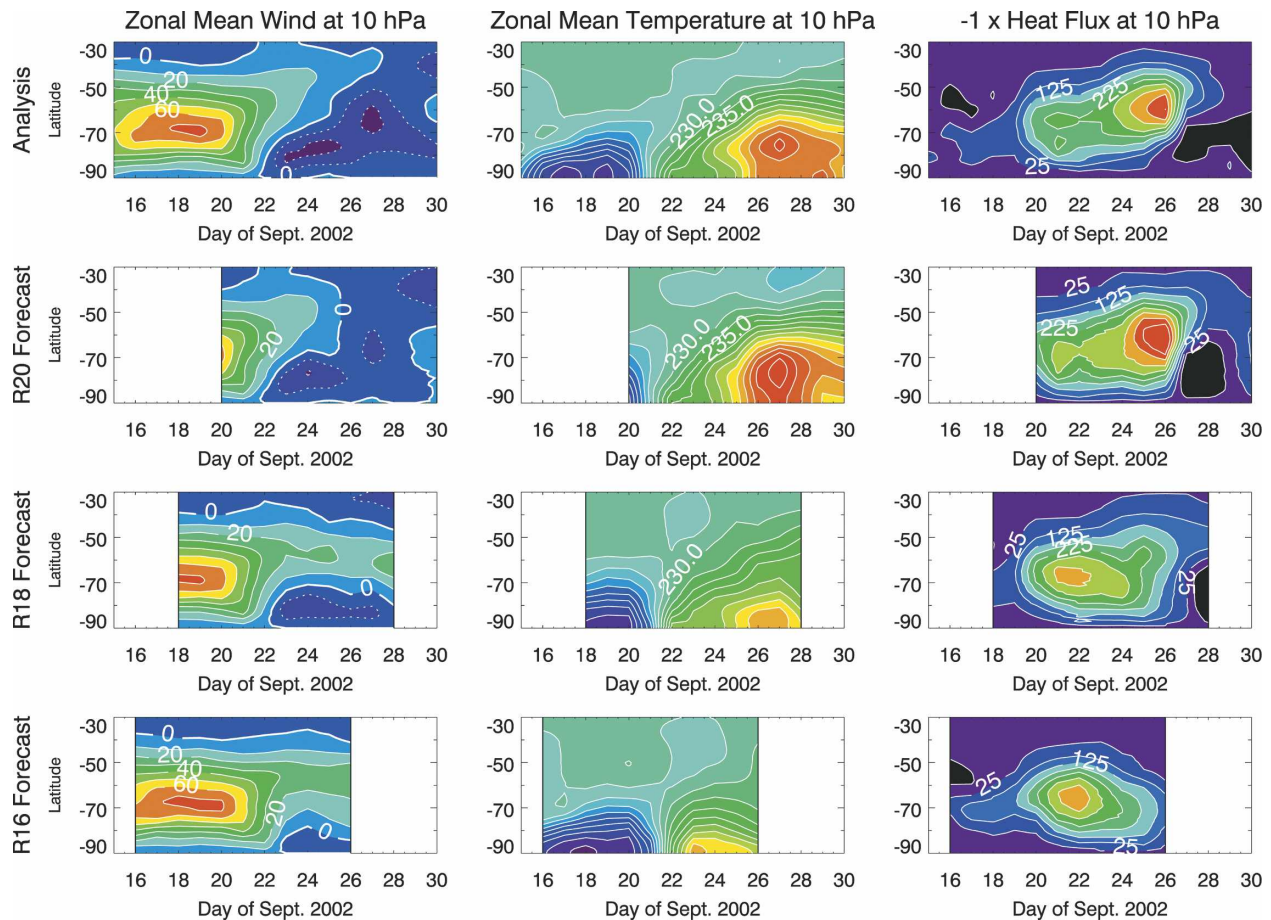


FIG. 3. (left) Zonal mean zonal wind, (middle) zonal mean temperature, and (right) zonal mean heat flux at 10 hPa for the period 15–30 Sep 2002. (top row) The analysis and (bottom three rows) the 10-day ALPHA-rean forecasts initialized 20, 18, and 16 Sep 2002.

warming following the reversal is underestimated in the R16 and R18 forecasts. The right column of Fig. 3 shows that the accompanying analyzed heat flux (here multiplied by  $-1$  to make poleward heat flux positive) strengthens from 18 to 26 September, peaks at around  $425 \text{ K m s}^{-1}$  near  $60^\circ\text{S}$ , then drops off rapidly. The heat flux for R20 matches the analyses well, with a very strong peak on 26 September, while R16 and R18 have heat fluxes that peak too early (22 September) and too weakly.

Figure 4 plots the evolution of geopotential height amplitudes of zonal wavenumbers at 10 hPa, along with the phase of the waves at  $60^\circ\text{S}$  (black circles). The analysis (top row) shows that wave 1 has a strong peak on 22 September, 4 days before the vortex split. From 22 to 26 September, the wave 1 amplitude decreases while waves 2 and 3 increase in amplitude. Wave 2 peaks at  $\sim 890 \text{ m}$ , while wave 3 peaks at  $\sim 670 \text{ m}$ . The large amplitudes of waves 2 and 3 are evident in the analyzed synoptic map for 26 September in Fig. 2. The phase progression shows wave 1 propagating slowly

eastward after 20 September, while waves 2 and 3 move rapidly eastward with brief stalling periods centered around 24 September.

The forecast wave evolution at 10 hPa in Fig. 4 shows that R20 captures well the amplitude and phase of these three large-scale waves. Results from both the R16 and R18 simulations show that the wave 1 amplitude persists too strongly following 22 September, since the analysis shows decay of wave 1 from 22 to 26 September. The wave 2 and wave 3 amplitudes for R16 and R18 show qualitatively similar evolution to the analyses, but the peak values are underestimated considerably. For example, the analyzed wave 3 peaks at  $667 \text{ m}$ , while R16 and R18 forecasts peak at  $397$  and  $553 \text{ m}$ , respectively. Although the amplitudes are weaker, R18 captures the phase evolution quite well up to 26 September, while R16 shows large errors in the wave 2 phase from 24 to 26 September. It is clear from Figs. 2, 3, and 4 that the longer forecasts (R16 and R18) underpredict the large wave 2 and 3 amplitudes that are necessary to produce a split vortex and reversal of the

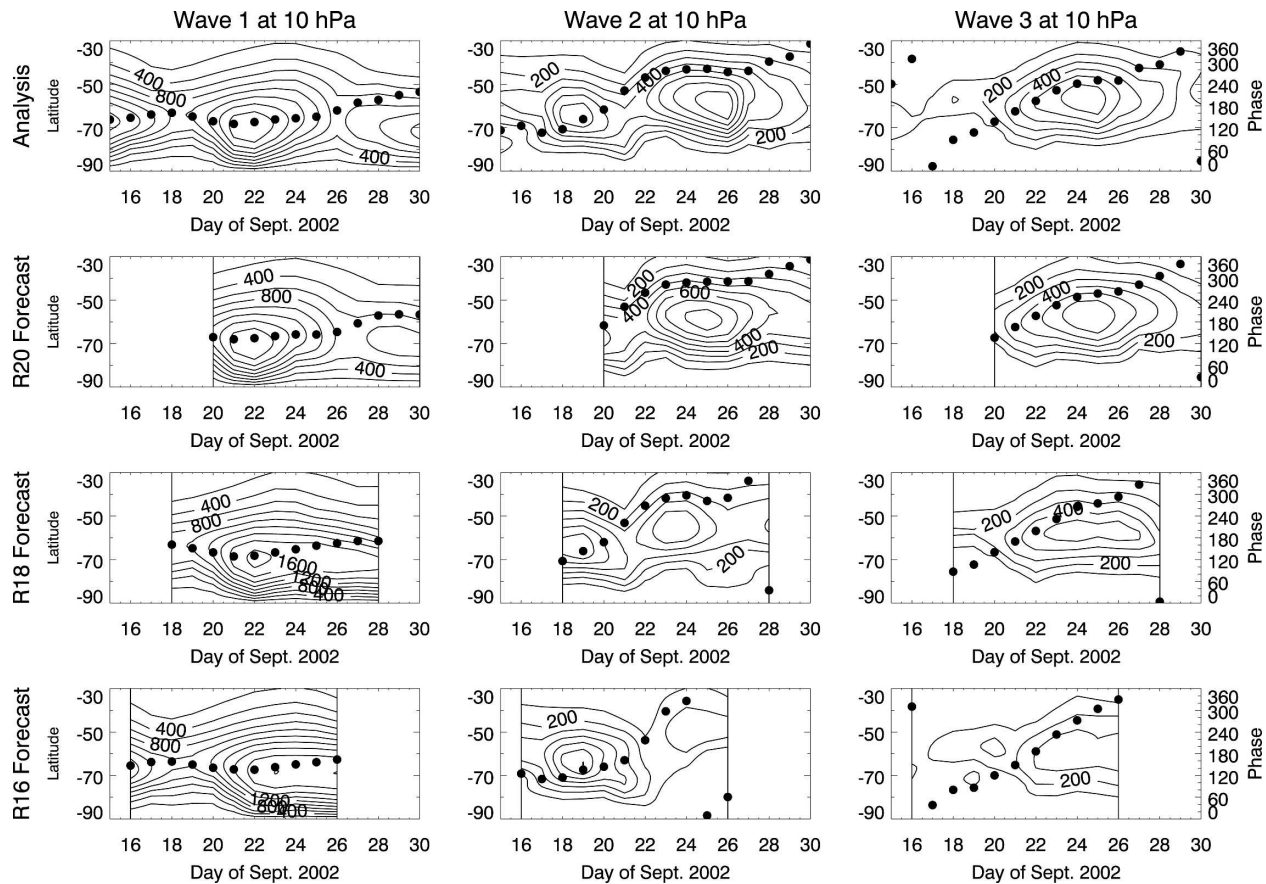


FIG. 4. Geopotential height amplitude of zonal wavenumbers (left) 1, (middle) 2, and (right) 3 at 10 hPa for the period 15–30 Sep 2002 along with the phase of these waves at 60°S (black circles). (top row) The analysis and (bottom three rows) the 10-day ALPHA-rean forecasts initialized 20, 18, and 16 Sep 2002. Contour labels are in meters.

winter jet. We now turn our attention to the lower stratosphere to examine the underlying wave forcing.

### c. Analyses and forecasts in the lower stratosphere (100 hPa)

Insight into the planetary wave forcing mechanisms for the 2002 SH major warming was provided by the mechanistic modeling study of Manney et al. (2005a), who examined the stratospheric response of the U.K. Universities Global Atmospheric Modeling Project (UGAMP) Stratosphere–Mesosphere Model (USMM) to geopotential height forcing at the lower boundary of 100 hPa. Their results showed strong sensitivity of the 10-hPa level to the 100-hPa boundary forcing, particularly to the low-wavenumber components. For example, when forced with only waves 1, 2, and 3, the model produced a major warming similar to observations. When only waves 1 and 2 were used, a strong warming occurred, but the vortex did not split com-

pletely, and the wind did not reverse at 60°S, 10 hPa (i.e., a major warming did not occur). Similarly, when wave 2 amplitudes were decreased, even by only 25%, a major warming did not occur. Interestingly, a major warming was produced when wave 1 was omitted and only waves 2 and 3 were included at 100 hPa. These results suggest that in order for a model to produce this major warming in the stratosphere, it must be able to accurately simulate the 100-hPa wave amplitudes, particularly waves 2 and 3.

The 100-hPa geopotential height maps from 16 to 23 September (not shown) indicate a nearly pole-centered vortex on 16 September, followed by rapid elongation of the polar vortex that develops a double-lobed structure by 24 September (Fig. 5), which is flanked by two opposing ridges on either side of the elongated vortex. This configuration results in very strong upward wave energy flux into the middle stratosphere (see below). The vortex does not completely split at 100 hPa; instead, the two cyclonic lobes merge together by 26 Sep-

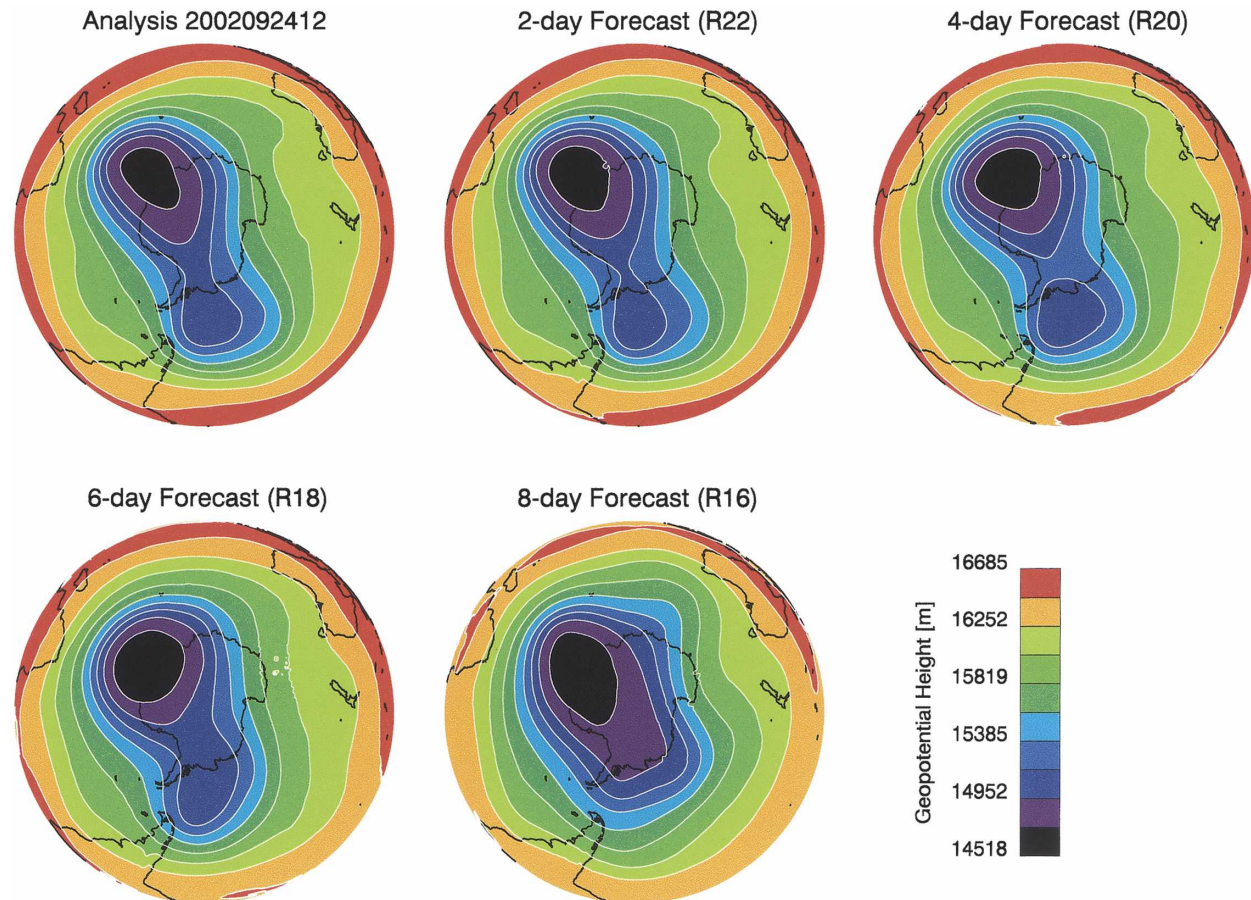


FIG. 5. Geopotential height at 100 hPa over the SH for 24 Sep 2002 for the analysis (NOGAPS reanalysis) and ALPHA-rean forecasts initialized 22, 20, 18, and 16 Sep 2002.

tember. R22 (2-day forecast) and R20 (4-day forecast) both show the vortex with a double-lobed shape, in agreement with the analysis. R18 (6-day forecast) shows somewhat less vortex elongation, while R16 (8-day forecast) completely fails to capture the double-lobed structure, yielding instead a much more compact, stable vortex.

These results are consistent with the evolution of the zonal mean wind at 100 hPa (Fig. 6, left column). The analyzed zonal wind decreases from a peak of around  $50 \text{ m s}^{-1}$  near  $60^\circ\text{S}$  to around  $10\text{--}20 \text{ m s}^{-1}$  by 22 September. R20, which was initialized at a time when the 100-hPa jet had already weakened considerably, shows good agreement with the analysis. R18 and R16 show weaker deceleration of the 100-hPa jet, with the jet for R16 remaining above  $20 \text{ m s}^{-1}$  at  $60^\circ\text{S}$ . The 100-hPa zonal mean temperatures are provided in Fig. 6 (middle column). The analysis shows a reversed gradient at polar latitudes starting around 23 September. The 100-hPa zonal mean temperature forecast for R20 shows rapid warming poleward of  $60^\circ\text{S}$ , but temperatures re-

main somewhat colder than the analyses. R16 and R18 show much weaker polar warming at this level and no reversal of the meridional gradient.

The analyzed 100-hPa heat flux (Fig. 6, top right) peaks on 22 September, several days before the 10-hPa heat flux reaches a maximum, indicating upward wave propagation. This strong peak was caused by simultaneous peaks in the heat flux contributions from waves 1, 2, and 3 (Newman and Nash 2005; Krüger et al. 2005; Harnik et al. 2005). As shown by Allen et al. (2003), this heat flux was much larger than that seen in any of the years from 1979 to 2002. The 100-hPa heat flux for R20 shows rapid growth from 20 to 22 September near  $60^\circ\text{S}$ , along with a secondary peak on 26 September near  $80^\circ\text{S}$ , consistent with a similar peak in the analyses. R18 and R16 also show growth near  $60^\circ\text{S}$ , but both underestimate the peak heat flux, with the R16 peak being considerably lower than the analyzed value. The underestimation of heat flux for R16 and R18 is clearly related to the reduced heat flux at 10 hPa and indicates weaker wave energy propagation throughout

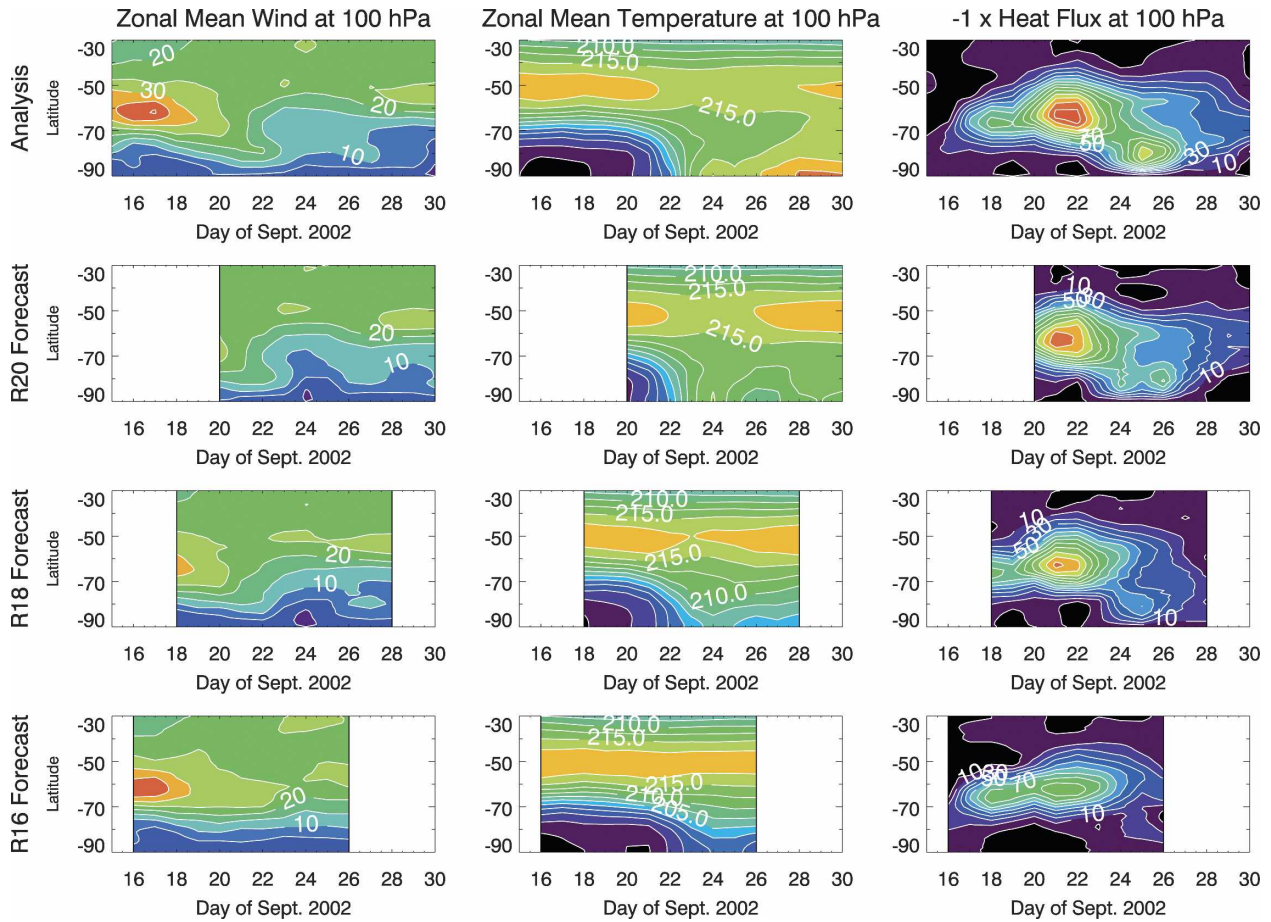


FIG. 6. Same as Fig. 3, but for 100 hPa.

the lower and middle stratosphere. To further diagnose how this relates to wave amplification we examine forecasts of the large-scale waves (Fig. 7).

At 100 hPa, the analysis shows wave 1 peaking around 20–22 September near 65°S, decaying for 2 days, and then slowly increasing through 30 September. Wave 2 peaks on 23 September near 60°S with very large amplitudes in excess of 450 m, while wave 3 peaks at over 150 m on 23–24 September. The strong growth rates of waves 2 and 3 at 100 hPa clearly play a major role in this event, as attested by the mechanistic modeling study of Manney et al. (2005a). The phase propagation of the waves at 100 hPa, 60°S indicates nearly stationary wave 1 and eastward propagation of waves 2 and 3, with a brief stalling period around 24 September, similar to that seen in the 10-hPa phases (Fig. 4). The superposition of eastward-propagating wave 2 and stationary wave 1 was shown by Harnik et al. (2005) to play a key role in the forcing of this major warming event. Harnik et al. (2005) further argued that the stratospheric wave 2 during this winter was enhanced

by anomalous poleward focusing and internal wave reflection, thereby increasing the likelihood of a combined wave 1 and 2 forcing event. In addition, Krüger et al. (2005) observed a correlation between amplification of the quasi-stationary wave 2 at 500 hPa with the amplification of the eastward-propagating wave 2 at 10 hPa 1–2 days later, throughout the 2002 winter, suggesting a tropospheric influence on the amplification of the stratospheric wave modes.

R20 captures the time evolution of the 100-hPa wave amplitudes and phases, although there are slight differences in the peak amplitudes between R20 and the analyses. R18 and R16 show excessively strong wave 1 amplitudes at 60°S from 20 to 26 September. This stronger wave 1 forcing at 100 hPa is consistent with the overestimation of the wave 1 for these runs at 10 hPa (Fig. 4). R18 does a fairly good job of capturing the wave 2 and 3 evolution, although again there are quantitative differences in the peak amplitudes, such as a weaker wave 2. R16, on the other hand, severely underestimates both wave 2 and wave 3 amplitudes, and

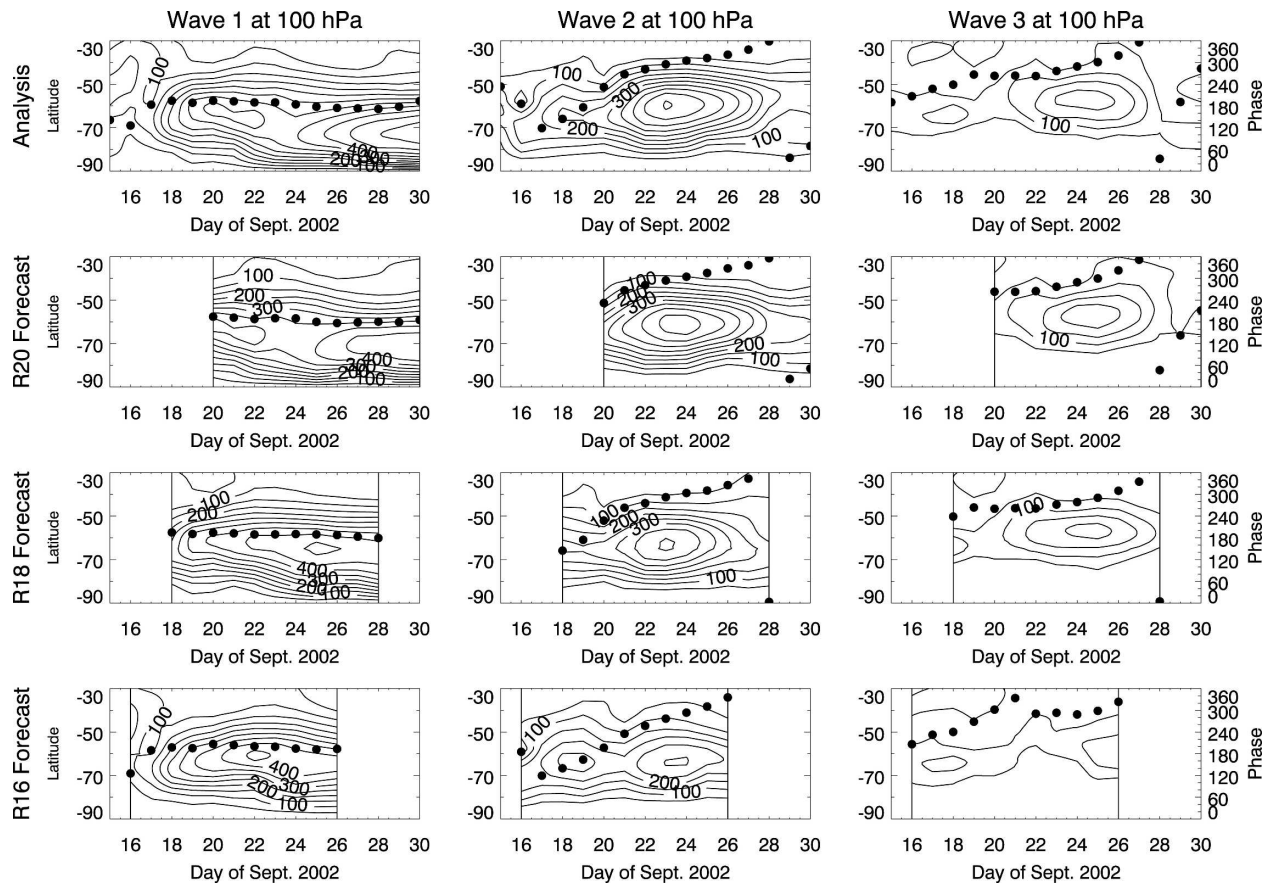


FIG. 7. Same as Fig. 4, but for 100 hPa.

shows rather large wave 3 phase errors around 21 September.

#### d. Analyses and forecasts in the troposphere (500 hPa)

We now examine the relationship between the stratospheric and tropospheric flow. Figure 8 provides synoptic maps of 500-hPa geopotential height for even-numbered days from 16 to 26 September. The tropospheric synoptic plots are more complex than those in the stratosphere, with significant activity at higher zonal wavenumbers that has not yet been filtered by the Charney and Drazin (1961) mechanism. As explained in NN04, a Rossby wave train developed in the troposphere during this period, originating from the western South Pacific and propagating eastward across the Western Hemisphere. Evidence of this wave train can be seen in Fig. 8 as a series of high and low anomalies extending over much of the Western Hemisphere (lower half of the plots). This wave train is consistent with the Pacific–South American blocking pattern discussed in Renwick and Revell (1999). NN04 docu-

mented a particularly strong blocking pattern, with a high over the South Atlantic and a low off the tip of South Africa. These features are identified in Fig. 8 by “H” and “L” for 20, 22, and 24 September. NN04 showed that the strength of this blocking feature (determined from differences in positive and negative geopotential height anomalies at 400 hPa) exceeded 3 times the local standard deviation of this quantity over 25 SH winters (1979–2003). Although the blocking was not necessarily the strongest observed during these years, it occurred during the weakest observed stratospheric polar night jet. It is likely that the unusual zonal mean flow associated with the weakened jet in 2002 facilitated the upward propagation of these waves (Harnik et al. 2005; Krüger et al. 2005; Newman and Nash 2005). NN04 also correlated this feature with strong upward flux of the wave activity diagnostic of Takaya and Nakamura (2001).

In Fig. 9, we show analyzed and 2- and 4-day forecasts of the 500-hPa geopotential height for 20 September, the approximate date of the South Atlantic blocking onset, along with the vertical component of the 3D

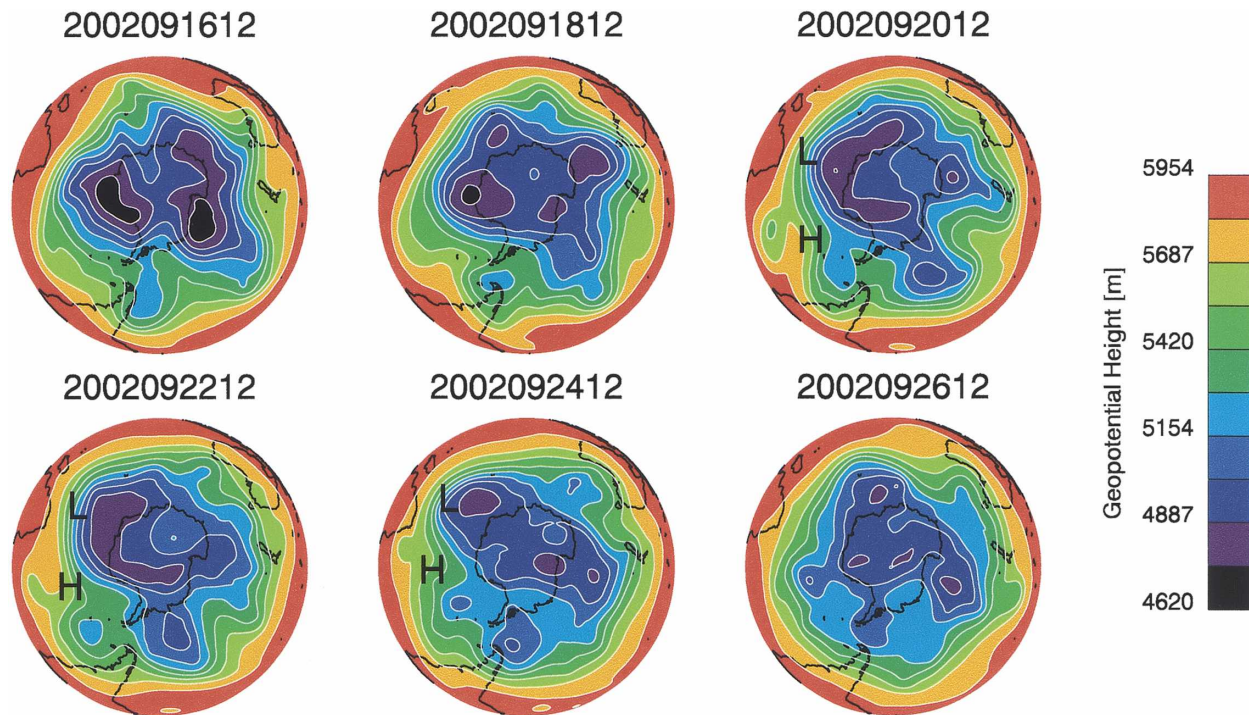


FIG. 8. Analyzed geopotential height at 500 hPa over the SH for 16–26 Sep 2002 (every other day).

EP flux averaged over the 5-day period 18–22 September at 500 hPa and 20–24 September at 100 hPa. The analyzed 500-hPa upward flux peaks at  $2.9 \text{ m}^2 \text{ s}^{-2}$  over the South Atlantic, at the location of the blocking high identified by NN04 (see “H” in Fig. 9). Secondary peaks occur over the western South Pacific, near New Zealand, and over the eastern South Pacific, off the coast of South America. These peaks in 3D EP flux are coincident with strong anticyclones seen in the 500-hPa geopotential heights, two of which occur in the preferred SH blocking regions (near Australia/New Zealand and South America) identified in previous observational studies (e.g., Trenberth and Mo 1985). Evidence of the upward extension of two of these features can be seen in the 100-hPa 3D EP-flux maps, which show large fluxes occurring over the South Atlantic and eastern South Pacific. A third peak occurs at 100 hPa, centered at  $90^\circ\text{E}$  longitude, and is not apparently connected with any 500-hPa feature.

The R18 and R16 forecasts of 500-hPa geopotential height on 20 September (Fig. 9, top) both show the blocking ridge over the South Atlantic and collocated peaks in the 500-hPa 3D EP flux. However, the South Atlantic ridge is somewhat weaker in the forecasts, particularly in R16 (4-day forecast). The 500-hPa 3D EP-flux maps for R18 and R16 show peak values over the South Atlantic of  $2.4$  and  $2.0 \text{ m}^2 \text{ s}^{-2}$ , respectively. The weakened ridges and associated heat fluxes, particu-

larly in R16, contribute to the more stable, circular polar vortex at 100 hPa (Fig. 5). The underprediction of upward 3D EP heat flux in the forecasts is even more dramatic at 100 hPa, with both R18 and R16 showing much weaker fluxes than the analyses. This is consistent with the underprediction of 100-hPa heat flux shown in Fig. 6.

NN04 argue that the wave activity originating from the South Atlantic ridge propagated energy upward into the middle stratosphere. This is confirmed in Fig. 10, which provides a vertical cross section of the 3D EP-flux vectors at  $50^\circ\text{S}$  (averaged from 18 to 22 September) plotted over the geopotential height zonal anomalies on 20 September. These flux vectors quantify propagation of planetary wave activity and reveal upward propagation of significant amounts of wave activity from the tropospheric ridge well into the stratosphere, with the stratospheric vectors progressively migrating eastward toward the Australian high at  $\sim 120^\circ\text{E}$ . The R18 forecast shows a similar pattern, although the magnitude of the flux vectors tends to be slightly weaker. The R16 forecast clearly underpredicts both the amplitude of the South Atlantic blocking high (seen by smaller geopotential height anomalies) and the strength of the upward propagating wave EP flux.

As discussed in section 2, previous work has shown that NWP models often have difficulty forecasting the onset and duration of tropospheric blocking in both the

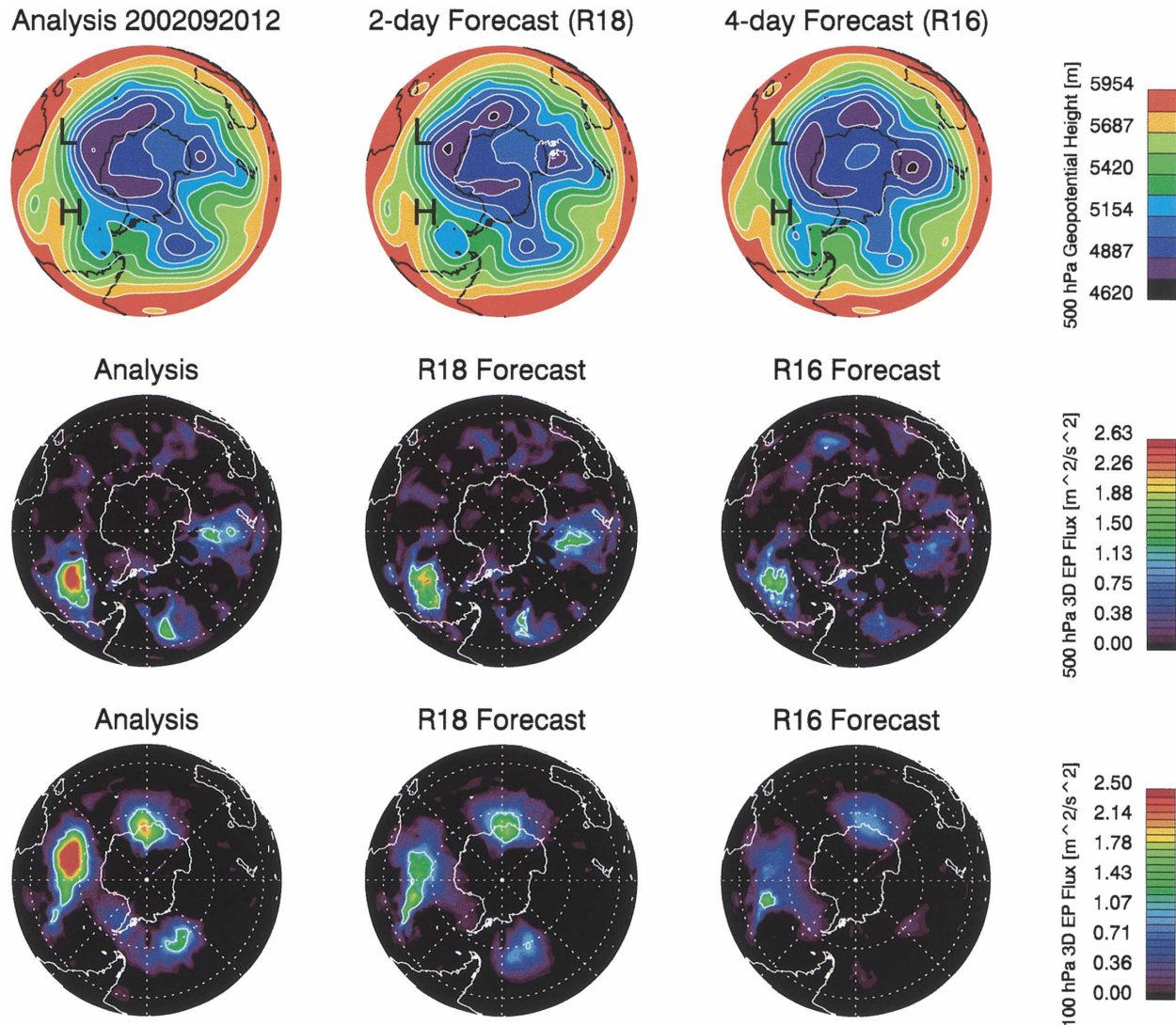


FIG. 9. (top row) Analyzed and ALPHA-rean (R18 and R16) forecasts of 500-hPa geopotential height for 20 Sep 2002. (middle) Analyzed and ALPHA-rean forecasts of the vertical component of 500-hPa 3D EP flux averaged from 18 to 22 Sep 2002. (bottom) Analyzed and ALPHA-rean forecasts of the vertical component of 100-hPa 3D EP flux averaged from 20 to 24 Sep 2002.

Northern and Southern Hemispheres (e.g., Tibaldi et al. 1994). In the case discussed here, it is clear that although R16 and R18 capture the location of the blocking, the predicted strength of the blocking and the associated upward-propagating planetary wave activity are both too weak. This clearly contributes to the weaker EP fluxes at 100 hPa around 23–24 September and decreased ability of NOGAPS-ALPHA to simulate the vortex splitting at 10 hPa around 25–26 September.

The 3D EP-flux patterns in Figs. 9 and 10 suggest launching of large-scale waves at 500 hPa. Figure 11 plots the analyzed and forecast wave amplitudes at this level. The analyzed wave 1 peaks near 60°S on 17 and

20 September, during the time of wave 1 growth at 100 hPa (Fig. 7). Waves 2 and 3 both have peaks around 23 September at 500 and 100 hPa. The phase propagation at 500 hPa leading up to the major warming (20–26 September) shows nearly stationary waves 1 and 2, and eastward propagating wave 3. Interestingly, there appears to be a short period around 20–22 September when the three waves are nearly in phase. This combination may have contributed to (or been a result of) the strong blocking patterns observed in Fig. 9.

The forecast wave amplitudes and phases at 500 hPa for R16, R18, and R20 are also shown in Fig. 11. R20 captures the decay of wave 1 and the growth and decay

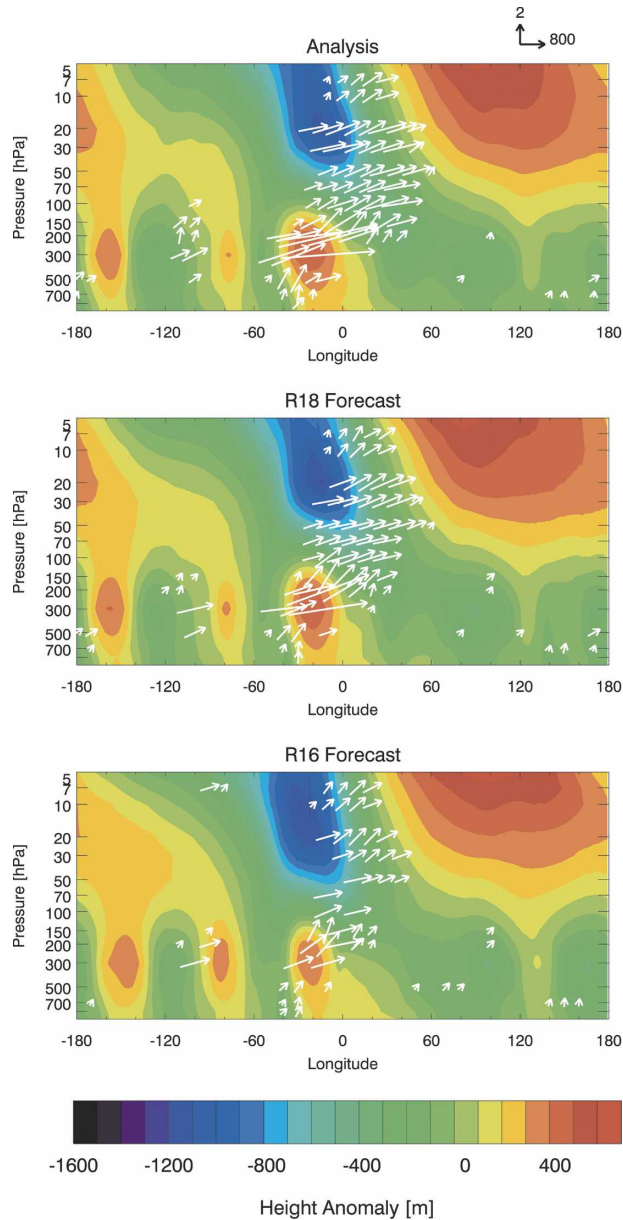


FIG. 10. Analyzed (top) and ALPHA-rean [(middle) R18 and (bottom) R16] forecasts of the cross section of geopotential height zonal anomalies at 50°S for 20 Sep 2002 overlaid with 3D EP-flux vectors at 50°S averaged from 18 to 22 Sep 2002. The vectors are in units  $\text{m}^2 \text{s}^{-2}$  with horizontal and vertical scaling lengths provided at top. Only vectors with vertical EP flux larger than  $0.8 \text{ m}^2 \text{s}^{-2}$  are plotted.

of waves 2 and 3 at 500 hPa as well as their phases up to 26 September. R18 also shows qualitatively the same features, but the peak wave amplitudes are quite different. For R16, the wave 1 amplitude is far too strong from 20 to 24 September near 60°S. This is consistent with excessive wave 1 amplitudes for this run at both 100 and 10 hPa. The R16 wave 2 peaks later than the

analyses, but with approximately the same amplitude, while the wave 3 does not show sufficient growth, consistent with the underestimated wave 3 growth at 100 hPa.

In summary, a comparison among new NOGAPS-ALPHA forecasts of the 2002 SH warming and meteorological analyses demonstrates a strong connection between the quality of the forecasts in the middle troposphere, lower stratosphere, and middle stratosphere. The strong planetary wave amplification in the middle stratosphere (10 hPa) is closely related to wave amplification in both the lower stratosphere (100 hPa) and the troposphere (500 hPa). Energy propagates upward from 500 hPa, particularly from a region of strong blocking over the South Atlantic. This blocking occurs on the leading edge of a Rossby wave train that spans the Western Hemisphere. However, the strength of the blocking may be enhanced by a brief in-phase relationship between waves 1, 2, and 3 at 500 hPa. The large amounts of upward-propagating wave energy cause extremely large heat fluxes and wave amplitudes at 100 hPa that in turn force the stratospheric major warming. Forecasts show that the earliest runs (R16 and R18) are unable to capture the strength of the blocking feature over the S. Atlantic. This results in weaker upward wave energy flux over the South Atlantic and a vortex that does not split. The R20 forecast was initialized at the peak of the 500-hPa heat flux and therefore did not have to forecast the onset of the blocking. This forecast resulted in much better heat fluxes and wave amplitudes at 100 hPa and a split middle-stratospheric vortex that agrees closely with analyses of the event.

#### 4. NOGAPS-ALPHA forecast skill assessment

A primary motivation for developing a high-altitude NWP model such as NOGAPS-ALPHA is to improve the system's overall forecast skill. Section 3 showed qualitatively that NOGAPS-ALPHA forecasts performed well out to 6 days in capturing the major features of the 2002 SH major warming. In this section we further quantify the improved forecast skill of NOGAPS-ALPHA in the SH using conventional forecast skill diagnostics. We examine NOGAPS-ALPHA forecasts initialized both with the reanalysis (ALPHA-rean) and with the operational "MVOI" NOGAPS analyses from 2002 (ALPHA-ops). We compare these with the archived operational 5-day NOGAPS forecasts made at the time (NOGAPS-ops).

To illustrate the differences among these three forecast models, we briefly examine 5-day forecasts valid on 26 September. Figure 12 plots the analyzed 10-hPa geopotential height along with 5-day forecasts initialized 21

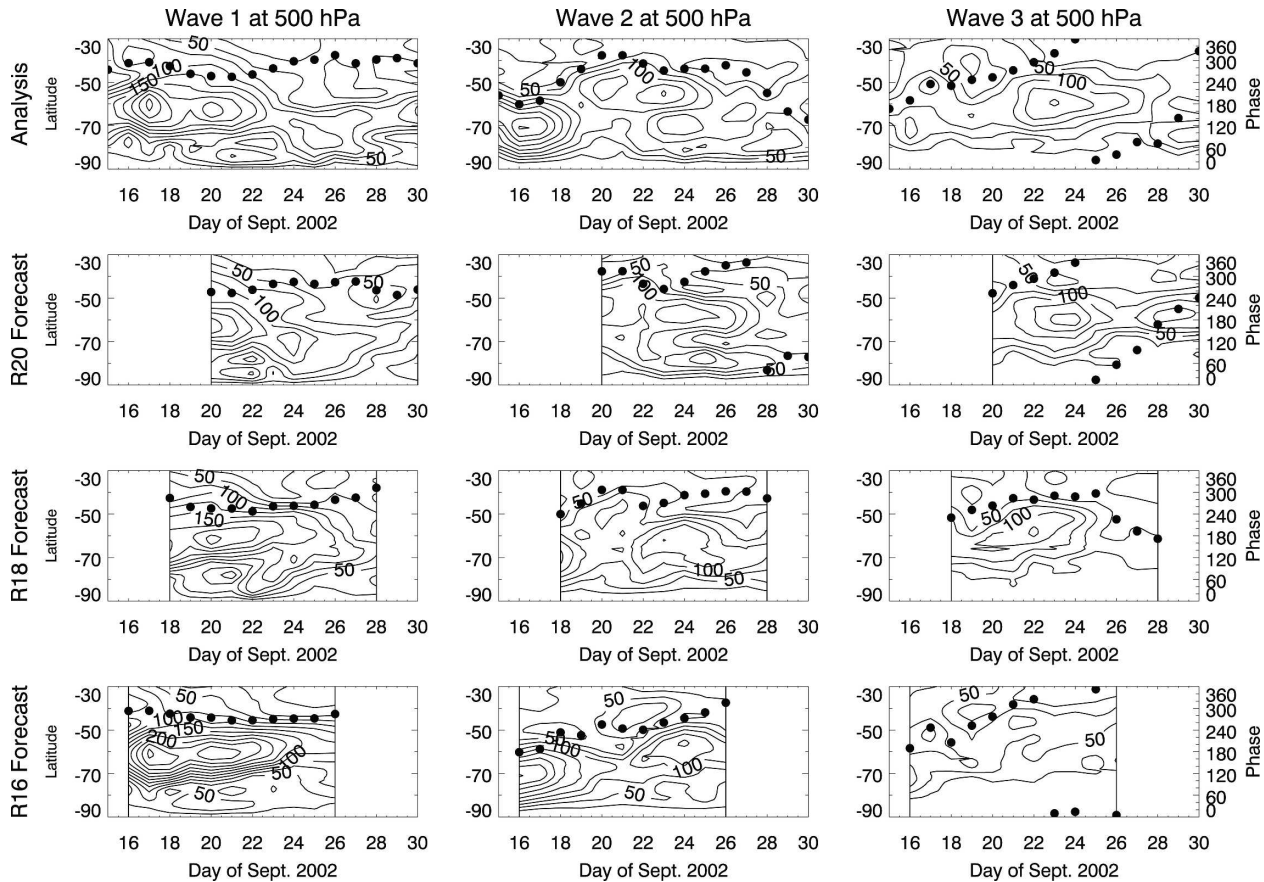


FIG. 11. Same as Fig. 4, but for 500 hPa.

September. The NOGAPS-ops forecast shows the vortex with two distinct lobes, but the vortex has not completely split. The ALPHA-ops forecast shows a definite splitting of the vortex, but the two lobes are not quite as widely separated as in the analyses. The ALPHA-rean forecast, on the other hand, captures the morphology of the split vortex very well, showing that the NAVDAS reanalysis provides an improvement over the MVOI analyses.

To assess more quantitatively the “skill” of these forecasts, we compare the models’ forecast wave amplitudes at 10 hPa with similarly computed diagnostics from seven different meteorological analyses. The range of analyzed values will provide some measure of the certainty to which the wave diagnostics are known, thereby providing a useful “truth range” to compare with the forecasts. In addition to the two Navy analyses (“ops” and “rean,” described in section 2), we also include analyses from the U.K. Meteorological Office (MetO), the NCEP/Climate Prediction Center (CPC) (NCEP/CPC), the ECMWF, NASA’s Goddard Earth Observing System (GEOS4), and the NCEP–National

Center for Atmospheric Research (NCAR) reanalysis (NCEP-REAN). The latter five analyses are described in detail in Manney et al. (2003, 2005b) and Randel et al. (2004).

The analyzed and 5-day forecast amplitudes for 26 September are plotted in Fig. 13. The top row shows the zonal wave 1, 2, and 3 amplitudes as a function of latitude for the seven analyses listed above. All analyses show wave 1 amplitudes that peak at over 650 m near  $65^{\circ}$ – $70^{\circ}$ S. There is some discrepancy among the analyses in the actual magnitude of the peak, particularly the NCEP-REAN and ops analyses, which peak higher and farther poleward than the other analyses. The wave 2 and 3 amplitudes both peak at  $60^{\circ}$ S with mean analyzed amplitudes near 850 and 575 m, respectively. The bottom row of Fig. 13 shows the corresponding 5-day forecasts of the wave amplitudes. The range of analyzed values in the upper plots is overlaid on these lower plots as the gray-shaded region, to aid comparison. For wave 1, NOGAPS-ops severely overpredicts the peak amplitude. Since the 10-hPa level lies within the NOGAPS-ops “sponge” layer region of enhanced numerical

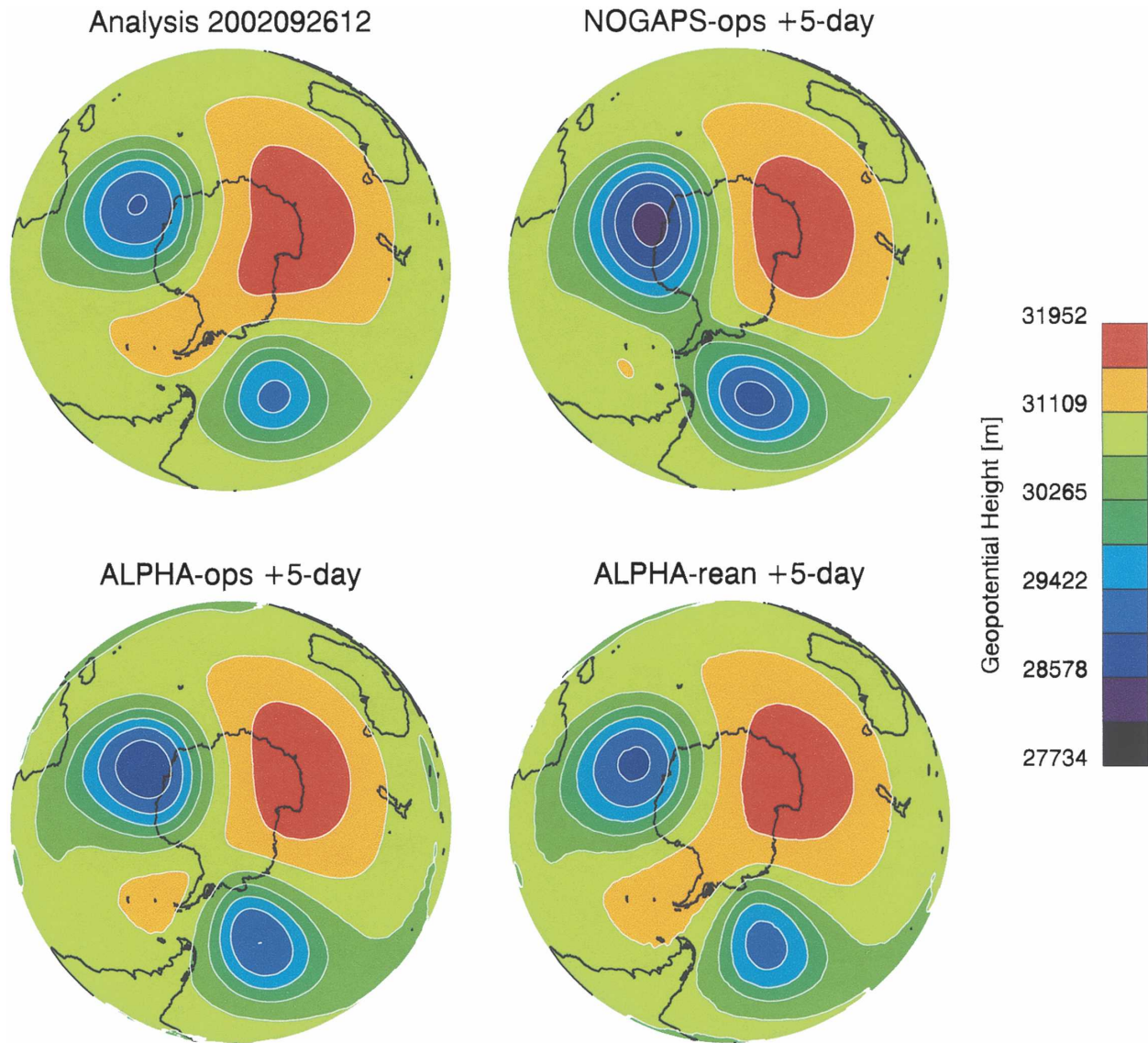


FIG. 12. Analyzed geopotential height at 10 hPa over the SH for 26 Sep 2002 along with the 5-day forecast geopotential height from NOGAPS-ops, ALPHA-ops, and ALPHA-rean. See section 2 for description of each model.

damping and vertical resolution is also rather poor here (see Fig. 1a), this is not too surprising. NOGAPS-ops forecast wave amplitudes lower down (30 and 50 hPa; not shown) are biased high, but not as severely as at 10 hPa. ALPHA-ops, which uses the same initial conditions, does a much better job with wave 1, although its forecast amplitude is still slightly too large. ALPHA-rean agrees quite well with the analysis, suggesting that the NAVDAS “rean” fields provide improved initial conditions over “ops” (MVOI). For wave 2, the ALPHA-ops and ALPHA-rean forecasts fall within the range of analyzed amplitudes, while the NOGAPS-ops forecast amplitude is slightly too low. For wave 3,

all forecast amplitudes are slightly larger than the analyses, with ALPHA-rean showing the best agreement.

These results show that for the 5-day forecast of the 2002 SH major warming, the ALPHA-rean and ALPHA-ops performed better than the NOGAPS-ops. As expected, the combination of an improved model and improved initial conditions yield improved forecasts. We now investigate whether the improvements found in this particular case point to more general improvements in SH forecast skill, both in the stratosphere and in the troposphere. To answer this, we quantify the average skill scores from forecasts initialized on even-

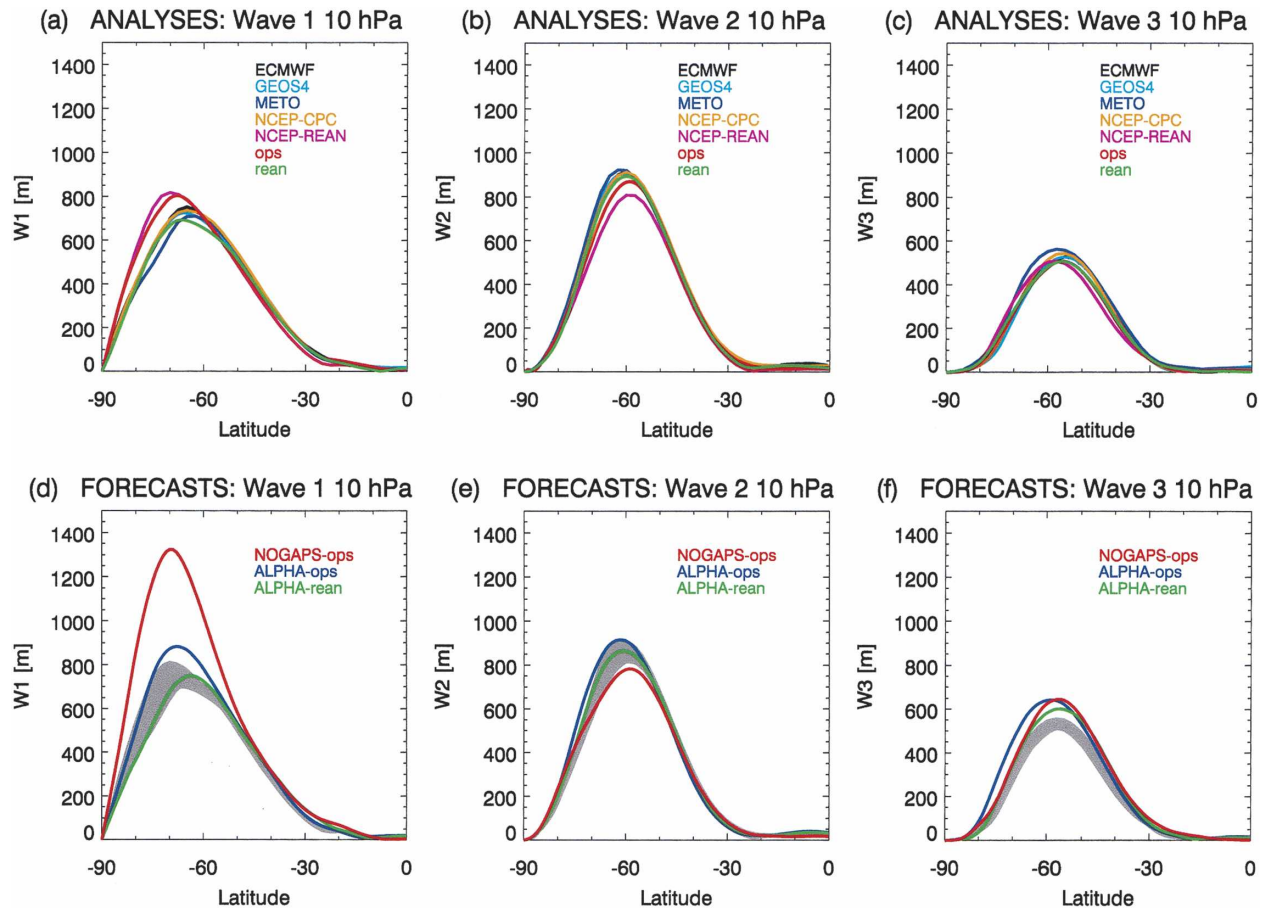


FIG. 13. Geopotential height zonal wave (left) 1, (middle) 2, and (right) 3 amplitudes at 10 hPa on 26 Sep 2002 over the SH for (a), (b), and (c) seven different analyses and (d), (e), (f) 5-day forecasts from NOGAPS-ops, ALPHA-ops, and ALPHA-rean. The shaded gray regions indicate the range of values from the seven analyses.

numbered days from 18 September to 10 October 2002. The skill diagnostic we use is the geopotential height anomaly correlation, evaluated over the latitude range  $20^{\circ}$ – $80^{\circ}$ S. This diagnostic has proven useful for assessing predictive skill in both the troposphere and stratosphere (e.g., Waugh et al. 1998; Lahoz 1999). The climatology used in this calculation is based on 25 yr (1980–2004) of NCEP-REAN geopotential heights.

Figure 14 plots the anomaly correlation (AC) at six pressure levels ranging from 10 to 500 hPa. ALPHA-ops forecasts show improved skill over NOGAPS-ops at all levels, with particularly large improvements occurring in the lower- to midstratosphere (50, 30, and 10 hPa). A Student's *t* test was performed to determine the significance of these calculated forecast differences. The improvements due to the new model (ALPHA-ops versus NOGAPS-ops) are significant (95% confidence level) at the 100-, 50-, 30-, and 10-hPa levels. The improvements at 200 and 500 hPa are significant at the 85% and 90% confidence levels, respectively.

ALPHA-rean shows an additional improvement over ALPHA-ops, with the AC differences between ALPHA-rean and NOGAPS-ops being significant (95% confidence level) at all pressures from 500 to 10 hPa. The 500-hPa AC, a standard tropospheric skill diagnostic, shows that ALPHA-rean forecasts have a 1-day improvement in forecast skill compared with NOGAPS-ops. The improvement is due to both the transitioning to the 3DVAR NAVDAS system and the introduction of Advanced Microwave Sounding Unit-A (AMSU-A) radiance assimilation. For further analysis of the impact of radiance assimilation on NOGAPS-ops forecast skill, see Baker et al. (2005). It is clear that using a forecast model with a higher top and improved treatment of middle-atmospheric photochemical and dynamical processes (NOGAPS-ALPHA), and introducing an improved analysis system (NAVDAS with radiance assimilation), will both positively impact the system's forecast skill in the Southern Hemisphere in the troposphere and stratosphere.

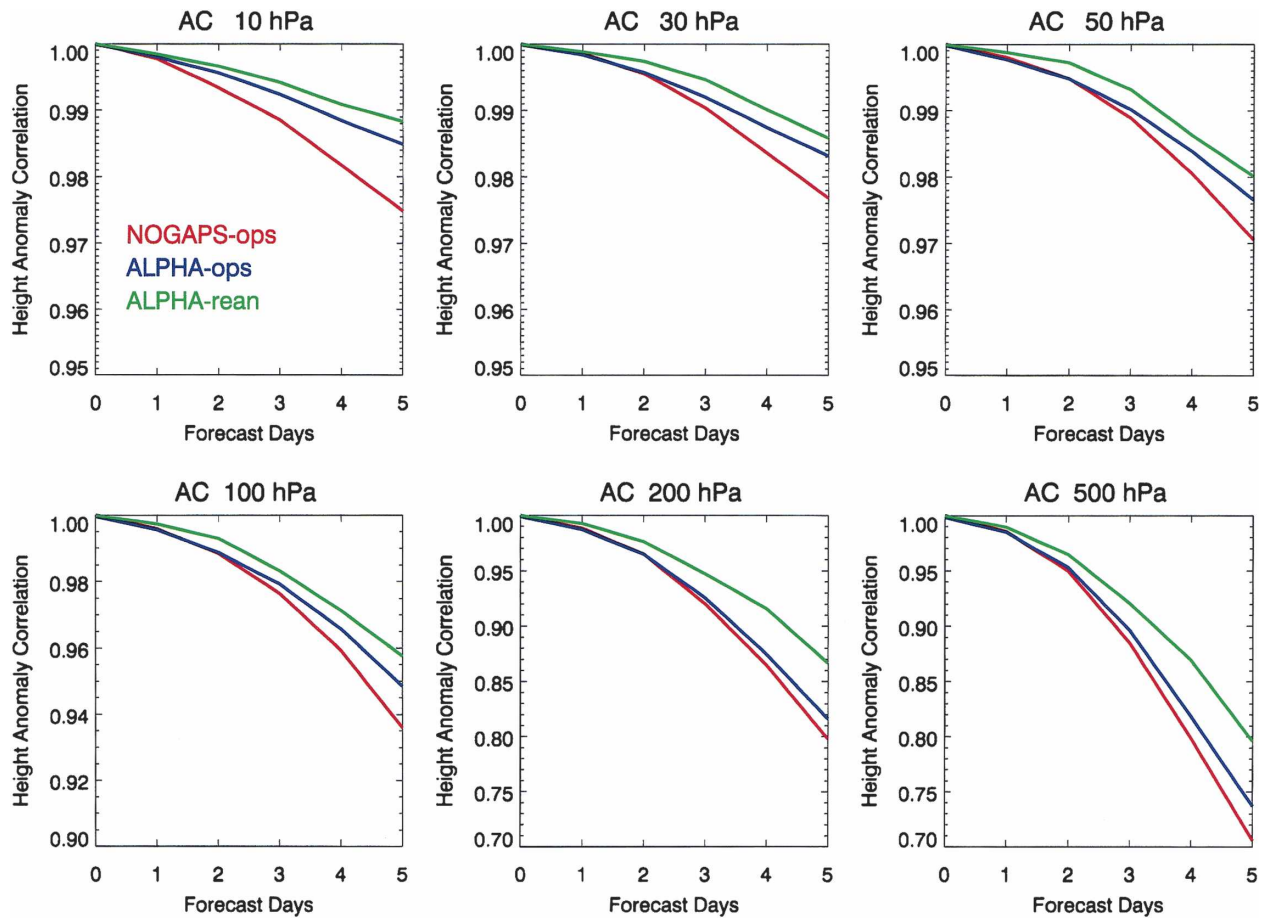


FIG. 14. Geopotential height anomaly correlation (calculated over  $20^{\circ}$ – $80^{\circ}$ S) at select pressure levels, averaged over forecasts initialized on even-numbered days from 18 Sep to 10 Oct 2002. The anomaly correlation is calculated with respect to the analysis used for initialization (i.e., rean for ALPHA-rean and ops for NOGAPS-ops and ALPHA-ops).

## 5. Summary/discussion

A new high-altitude version of the NOGAPS forecast model (NOGAPS-ALPHA) has been developed and was used to simulate the September 2002 SH stratospheric major warming. While forecasts out to 6 days were able to capture the main features of the event, longer forecasts (8 and 10 days) could not produce the observed split vortex and wind reversal at 10 hPa. This was due to the inability of the longer forecasts to correctly predict the strength of a tropospheric blocking ridge over the South Atlantic, which launched large-amplitude planetary waves into the stratosphere. Forecasts of less than 6 days were initialized with the blocking in place, and therefore did not need to simulate the blocking onset.

Why were the longer forecasts unable to capture the magnitude of the blocking? Numerous studies have examined in detail the ability (or inability) of NWP mod-

els to forecast blocking onset, duration, and decay (e.g., Tibaldi and Molteni 1990; Tibaldi et al. 1994). The skill of forecasting blocks tends to exhibit large case-to-case variability, and it can be very difficult to identify why particular forecasts break down. In this case, Niishi and Nakamura (2004) argue that the original source of the Rossby wave train that developed the South Atlantic block was strong convection over the South Pacific convergence zone. Future studies of this event would benefit from examining the sensitivity of the blocking development to the quality of the parameterization and analysis of the convective source region. In addition, further examination of the combined roles of the observed blocking patterns, the in-phase relationship of 500-hPa geopotential height zonal waves 1, 2, and 3, and the vertical wave propagation characteristics is warranted.

Conventional skill diagnostics were used to quantify NOGAPS-ALPHA forecast skill in both the tropo-

sphere and stratosphere based on 3 weeks of forecasts in September–October 2002. NOGAPS-ALPHA forecasts initialized with NOGAPS operational analyses (ALPHA-ops) showed an improvement over NOGAPS-ops at all levels from 700 to 10 hPa. These improvements are likely due to a combination of 1) better vertical coordinate: hybrid sigma pressure rather than pure sigma; 2) better vertical resolution in the stratosphere; 3) higher model top; and 4) improved radiation scheme. Model topography also affects the magnitude of quasi-stationary planetary waves (Kim and Hogan 2004) and synoptic-scale blocking (e.g., Mullen 1994). Since the current NOGAPS-ops uses mean orography instead of the silhouette orography that was used in this study, this may have an impact on the forecast of the major warming.

A more significant improvement over NOGAPS-ops occurred when ALPHA runs were initialized with a reanalysis based on an improved assimilation system (ALPHA-rean). The analysis improvements included 1) using a 3D variational scheme rather than the then-operational multivariate optimal interpolation and 2) using AMSU-A radiances rather than retrieved temperature profiles. These ALPHA-rean forecasts yielded wave amplitudes in the middle stratosphere that were much closer to the consensus range of various analyses. Forecast skill calculations showed a significant positive impact of the reanalysis on forecast skill from 10 to 500 hPa. The improvements in forecast skill reported here therefore result from both a better forecast model and a better analysis for initialization. The improvements to the assimilation scheme have already been transitioned to operations at FNMOC (NAVDAS in October 2003; AMSU-A radiance assimilation in June 2004). We are currently planning further tests of and improvements to the NOGAPS-ALPHA forecast model. The goal is to progressively transition aspects of the NOGAPS-ALPHA upgrades to the operational forecast model at FNMOC.

*Acknowledgments.* This work was supported in part by the Office of Naval Research through the Naval Research Laboratory's base 6.2 program, by the National Aeronautics and Space Administration (NASA) Geospace Sciences Program, and by an Internal Government Study from the Integrated Program Office of the National Polar Orbiting Environmental Satellite System (NPOESS). Computing resources were provided by the Department of Defense High Performance Computing Modernization Program at the U.S. Army Space & Missile Defense Command (SMDC) Simulation Center. Work at the Jet Propulsion Laboratory,

California Institute of Technology, was performed under contract with the NASA.

#### REFERENCES

- Allen, D. R., R. M. Bevilacqua, G. E. Nedoluha, C. E. Randall, and G. L. Manney, 2003: Unusual stratospheric transport and mixing during the 2002 Antarctic winter. *Geophys. Res. Lett.*, **30**, 1599, doi:10.1029/2003GL017117.
- Andrews, D. G., J. R. Holton, and C. B. Leovy, 1987: *Middle Atmosphere Dynamics*. Academic Press, 489 pp.
- Baker, N. L., T. F. Hogan, W. F. Campbell, R. L. Pauley, and S. D. Swadley, 2005: The impact of AMSU-A radiance assimilation in the U.S. Navy's Operational Global Atmospheric Prediction System (NOGAPS). Naval Research Laboratory Rep. NRL/MR/7530-05-8836, 22 pp.
- Baldwin, M. P., T. Hirooka, A. O'Neill, and S. Yoden, 2003: Major stratospheric warming in the Southern Hemisphere in 2002: Dynamical aspects of the ozone hole split. *SPARC Newsletter*, No. 20, World Climate Research Program, 24–26.
- Cariolle, D., and M. Déqué, 1986: Southern Hemisphere medium-scale waves and total ozone disturbances in a spectral general circulation model. *J. Geophys. Res.*, **91**, 10 825–10 846.
- Charney, J. G., and P. G. Drazin, 1961: Propagation of planetary scale disturbances from the lower into the upper atmosphere. *J. Geophys. Res.*, **66**, 83–109.
- Chou, M.-D., and M. J. Suarez, 2002: A solar radiation parameterization for atmospheric studies. NASA Tech. Memo. 10460, Vol. 15, Technical Report Series on Global Modeling and Data Assimilation, 52 pp.
- , —, X. Z. Liang, and M.-H. Yan, 2001: A thermal infrared radiation parameterization for atmospheric studies. NASA Tech. Memo. 104606, Vol. 19, Technical Report Series on Global Modeling and Data Assimilation, 65 pp.
- Coy, L., D. E. Siskind, S. E. Eckermann, J. P. McCormack, D. R. Allen, and T. F. Hogan, 2005: Modeling the August 2002 minor warming event. *Geophys. Res. Lett.*, **32**, L07808, doi:10.1029/2005GL022400.
- Daley, R., and E. Barker, 2001: NAVDAS: Formulation and diagnostics. *Mon. Wea. Rev.*, **129**, 869–883.
- Eckermann, S. D., J. P. McCormack, L. Coy, D. Allen, T. Hogan, and Y.-J. Kim, 2004: NOGAPS-ALPHA: A prototype high-altitude global NWP model. Preprints, *Symp. on the 50th Anniversary of Operational Numerical Weather Prediction*, College Park, MD, Amer. Meteor. Soc., P2.6.
- Emanuel, K. A., and M. Zivkovic-Rothman, 1999: Development and evaluation of a convection scheme for use in climate models. *J. Atmos. Sci.*, **56**, 1766–1782.
- Errico, R. M., E. H. Barker, and R. Gelaro, 1988: A determination of balanced normal modes for two models. *Mon. Wea. Rev.*, **116**, 2717–2724.
- Fleming, E. L., S. Chandra, J. J. Barnett, and M. Corney, 1990: Zonal mean temperature, pressure, zonal wind, and geopotential height as functions of latitude, COSPAR International Reference Atmosphere: 1986, Part II: Middle atmosphere models. *Adv. Space Res.*, **10** (12), 11–59.
- Goerss, J., and P. Phoebus, 1992: The Navy's operational atmospheric analysis. *Wea. Forecasting*, **7**, 232–249.
- Harnik, N., R. K. Scott, and J. Perlwitz, 2005: Wave reflection and focusing prior to the major stratospheric warming of September 2002. *J. Atmos. Sci.*, **62**, 640–650.
- Harshvardhan, R. Davies, D. Randall, and T. Corsetti, 1987: A fast radiation parameterization for atmospheric circulation models. *J. Geophys. Res.*, **92**, 1009–1016.

- Harvey, V. L., R. B. Pierce, T. D. Fairlie, and M. H. Hitchman, 2002: A climatology of stratospheric polar vortices and anticyclones. *J. Geophys. Res.*, **107**, 4442, doi:10.1029/2001JD001471.
- Hogan, T., and T. Rosmond, 1991: The description of the Navy Operational Global Atmospheric Prediction System's spectral forecast model. *Mon. Wea. Rev.*, **119**, 1786–1815.
- , —, and R. Gelaro, 1991: The NOGAPS forecast model: A technical description. Naval Oceanographic and Atmospheric Research Laboratory Rep. 13, 219 pp.
- Kim, Y.-J., and T. F. Hogan, 2004: Response of a global atmospheric forecast model to various drag parameterizations. *Tellus*, **56A**, 472–484.
- Krüger, K., B. Naujokat, and K. Labitzke, 2005: The unusual mid-winter warming in the Southern Hemisphere stratosphere 2002: A comparison to Northern Hemisphere phenomena. *J. Atmos. Sci.*, **62**, 603–613.
- Lahoz, W. A., 1999: Predictive skill of the UKMO Unified Model in the lower stratosphere. *Quart. J. Roy. Meteor. Soc.*, **125**, 2205–2238.
- Louis, J. F., 1979: A parametric model of vertical eddy fluxes in the atmosphere. *Bound.-Layer Meteor.*, **17**, 187–202.
- , M. Tiedtke, and J. F. Geleyn, 1982: A short history of the operational PBL parameterization at ECMWF. *Proc. ECMWF Workshop on Planetary Boundary Parameterizations*, Reading, United Kingdom, ECMWF, 59–79.
- Manney, G. L., J. L. Sabutis, S. Pawson, M. L. Santee, B. Naujokat, R. Swinbank, M. E. Gelman, and W. Ebisuzaki, 2003: Lower stratospheric temperature differences between meteorological analyses in two cold Arctic winters and their impact on polar processing studies. *J. Geophys. Res.*, **108**, 8328, doi:10.1029/2001JD001149.
- , and Coauthors, 2005a: Simulations of dynamics and transport during the September 2002 Antarctic major warming. *J. Atmos. Sci.*, **62**, 690–707.
- , and Coauthors, 2005b: Diagnostic comparison of meteorological analyses during the 2002 Antarctic winter. *Mon. Wea. Rev.*, **133**, 1261–1278.
- McCormack, J. P., and Coauthors, 2004: NOGAPS-ALPHA model simulations of stratospheric ozone during the SOLVE2 campaign. *Atmos. Chem. Phys.*, **4**, 2401–2423.
- McLinden, C. A., S. C. Olsen, B. Hanneegan, O. Wild, M. J. Prather, and J. Sundet, 2000: Stratospheric ozone in 3-D models: A simple chemistry and the cross-tropopause flux. *J. Geophys. Res.*, **105**, 14 653–14 665.
- Mechoso, C. R., K. Yamazaki, A. Kitoh, and A. Arakawa, 1985: Numerical forecasts of stratospheric warming events during the winter of 1979. *Mon. Wea. Rev.*, **113**, 1015–1029.
- , M. J. Suarez, K. Yamazaki, A. Kitoh, and A. Arakawa, 1986: Numerical forecasts of tropospheric and stratospheric events during the winter of 1979: Sensitivity to the model's horizontal resolution and vertical extent. *Advances in Geophysics*, Vol. 29, Academic Press, 375–413.
- , A. O'Neill, V. D. Pope, and J. D. Farrara, 1988: A study of the stratospheric final warming of 1982 in the Southern Hemisphere. *Quart. J. Roy. Meteor. Soc.*, **114**, 1365–1384.
- Mukougawa, H., and T. Hirooka, 2004: Predictability of stratospheric sudden warming: A case study for 1998/99 winter. *Mon. Wea. Rev.*, **132**, 1764–1776.
- Mullen, S. L., 1994: The impact of an envelope orography on low-frequency variability and blocking in a low-resolution general circulation model. *J. Climate*, **7**, 1815–1826.
- Newman, P. A., and E. R. Nash, 2005: The unusual Southern Hemisphere winter of 2002. *J. Atmos. Sci.*, **62**, 614–628.
- Niishi, K., and H. Nakamura, 2004: The tropospheric origin of the diminished Antarctic ozone hole in September 2002. *Geophys. Res. Lett.*, **31**, L16103, doi:10.1029/2004GL019532.
- Palmer, T. N., G. J. Shutts, and R. Swinbank, 1986: Alleviation of a systematic westerly bias in general circulation and numerical weather prediction models through an orographic gravity wave drag parameterization. *Quart. J. Roy. Meteor. Soc.*, **112**, 1001–1039.
- Peng, M. S., J. A. Ridout, and T. F. Hogan, 2004: Recent modifications of the Emanuel convective scheme in the Navy Operational Global Atmospheric Prediction System. *Mon. Wea. Rev.*, **132**, 1254–1268.
- Plumb, R. A., 1986: Three-dimensional propagation of transient quasi-geostrophic eddies and its relationship with the eddy forcing of the time-mean flow. *J. Atmos. Sci.*, **43**, 1657–1678.
- Quiroz, R. S., 1986: The association of stratospheric warming with tropospheric blocking. *J. Geophys. Res.*, **91**, 5277–5285.
- Randel, W. J., and Coauthors, 2004: The SPARC intercomparison of middle atmosphere climatologies. *J. Climate*, **17**, 986–1003.
- Renwick, J. A., and M. J. Revell, 1999: Blocking over the South Pacific and Rossby wave propagation. *Mon. Wea. Rev.*, **127**, 2233–2247.
- Riishojgaard, L. P., I. Stajner, and G. P. Lou, 2000: The GEOS ozone data assimilation system. *Adv. Space Res.*, **25**, 1063–1072.
- Scaife, A. A., D. R. Jackson, R. Swinbank, N. Butchard, H. E. Thornton, M. Keil, and L. Henderson, 2005: Stratospheric vacillations and the major warming over Antarctica in 2002. *J. Atmos. Sci.*, **62**, 629–639.
- Simmons, A., M. Hortal, G. Kelly, A. McNally, A. Untch, and S. Uppala, 2005: ECMWF analyses and forecasts of stratospheric winter polar vortex break-up: September 2002 in the Southern Hemisphere and related events. *J. Atmos. Sci.*, **62**, 668–689.
- Sinnhuber, B.-M., M. Weber, A. Amankwah, and J. P. Burrows, 2003: Total ozone during the unusual Antarctic winter of 2002. *Geophys. Res. Lett.*, **30**, 1581, doi:10.1029/2003GL017086.
- Slingo, J. M., 1987: The development and verification of a cloud prediction scheme in the ECMWF model. *Quart. J. Roy. Meteor. Soc.*, **113**, 899–927.
- Stajner, I., L. P. Riishojgaard, and R. B. Rood, 2001: The GEOS ozone data assimilation system: Specification of error statistics. *Quart. J. Roy. Meteor. Soc.*, **127**, 1069–1094.
- Swinbank, R., and D. A. Ortland, 2003: Compilation of wind data for the Upper Atmosphere Research Satellite (UARS) reference atmosphere project. *J. Geophys. Res.*, **108**, 4615, doi:10.1029/2002JD003135.
- Takaya, K., and H. Nakamura, 2001: A formulation of phase-independent wave-activity flux for stationary and migratory quasi-geostrophic eddies on a zonally varying basic flow. *J. Atmos. Sci.*, **58**, 608–627.
- Teixeira, J., and T. Hogan, 2002: Boundary layer clouds in a global atmospheric model: Simple cloud cover parameterization. *J. Climate*, **15**, 1261–1276.
- Tibaldi, S., and F. Molteni, 1990: On the operational predictability of blocking. *Tellus*, **42A**, 343–365.
- , E. Tosi, A. Navarra, and L. Pedulli, 1994: Northern and Southern Hemisphere seasonal variability of blocking frequency and predictability. *Mon. Wea. Rev.*, **122**, 1971–2003.
- Tiedtke, M., 1984: The sensitivity of the time-scale flow to cumulus convection in the ECMWF model. *Proc. Workshop on*

- Large-Scale Numerical Models*, Reading, United Kingdom, ECMWF, 297–316.
- Trenberth, K. E., and K. C. Mo, 1985: Blocking in the Southern Hemisphere. *Mon. Wea. Rev.*, **113**, 3–21.
- , and D. P. Stepaniak, 2002: A pathological problem with NCEP reanalyses in the stratosphere. *J. Climate*, **15**, 690–695.
- Waugh, D. W., J. M. Sisson, and D. J. Karoly, 1998: Predictive skill of an NWP system in the southern lower stratosphere. *Quart. J. Roy. Meteor. Soc.*, **124**, 2181–2200.
- Weber, M., S. Dhomse, F. Wittrock, A. Richter, B.-M. Sinnhuber, and J. P. Burrows, 2003: Dynamical control of NH and SH winter/spring total ozone from GOME observations in 1995–2002. *Geophys. Res. Lett.*, **30**, 1583, doi:10.1029/2002GL016799.
- Webster, S., A. R. Brown, D. R. Cameron, and C. P. Jones, 2003: Improvements to the representation of orography in the Met Office Unified Model. *Quart. J. Roy. Meteor. Soc.*, **129**, 1989–2010.